♻EPA **Research and Development**

METHANE-STEAM REACTION

OVER NICKEL CATALYSTS

IN THE HYNOL PROCESS

Prepared for

National Risk Management Research Laboratory

Prepared by

**National Risk Management
Research Laboratory
Research Triangle Park, NC 27711**

METHANE-STEAM REACTION OVER NICKEL CATALYSTS

IN THE HYNOL PROCESS

Prepared by:

Yuanji Dong and Jarek Karwowski
Acurex Environmental Corporation
4915 Prospectus Drive
P.O. Box 13109
Research Triangle Park, NC 27709

Project Officer: Robert H. Borgwardt
U.S. Environmental Protection Agency
National Risk Management Research Laboratory
Air Pollution Prevention and Control Division
Atmospheric Protection Branch
Research Triangle Park, NC 27711

Prepared for:

U.S. Environmental Protection Agency
Office of Research and Development
Washington, D.C. 20460

FOREWORD

The U.S. Environmental Protection Agency is charged by Congress with protecting the Nation's land, air, and water resources. Under a mandate of national environmental laws, the Agency strives to formulate and implement actions leading to a compatible balance between human activities and the ability of natural systems to support and nurture life. To meet this mandate, EPA's research program is providing data and technical support for solving environmental problems today and building a science knowledge base necessary to manage our ecological resources wisely, understand how pollutants affect our health, and prevent or reduce environmental risks in the future.

The National Risk Management Research Laboratory is the Agency's center for investigation of technological and management approaches for reducing risks from threats to human health and the environment. The focus of the Laboratory's research program is on methods for the prevention and control of pollution to air, land, water, and subsurface resources; protection of water quality in public water systems; remediation of contaminated sites and groundwater; and prevention and control of indoor air pollution. The goal of this research effort is to catalyze development and implementation of innovative, cost-effective environmental technologies; develop scientific and engineering information needed by EPA to support regulatory and policy decisions; and provide technical support and information transfer to ensure effective implementation of environmental regulations and strategies.

This publication has been produced as part of the Laboratory's strategic long-term research plan. It is published and made available by EPA's Office of Research and Development to assist the user community and to link researchers with their clients.

> E. Timothy Oppelt, Director
> National Risk Management Research Laboratory

EPA REVIEW NOTICE

PB98-100480

1. REPORT NO.	2.	3
EPA-600/R-97-093		

4. TITLE AND SUBTITLE	5. REPORT DATE
Methane-Steam Reaction Over Nickel Catalysts in the Hynol Process	September 1997
	6. PERFORMING ORGANIZATION CODE

7. AUTHOR(S)	8. PERFORMING ORGANIZATION REPORT NO.
Yuanji Dong and Jarek Karwowski	

9. PERFORMING ORGANIZATION NAME AND ADDRESS	10. PROGRAM ELEMENT NO.
Acurex Environmental Corporation P. O. Box 13109 Research Triangle Park, North Carolina 27709	11. CONTRACT/GRANT NO. 68-D4-0005, WAs 2-032 and 3-019

12. SPONSORING AGENCY NAME AND ADDRESS	13. TYPE OF REPORT AND PERIOD COVERED
EPA, Office of Research and Development Air Pollution Prevention and Control Division Research Triangle Park, NC 27711	Final; 10/95 - 4/97
	14. SPONSORING AGENCY CODE EPA/600/13

15. SUPPLEMENTARY NOTES APPCD project officer is Robert H. Borgwardt, Mail Drop 63, 919/541-2336.

16. ABSTRACT The report discusses the reaction of methane-steam over nickel catalysts in the Hynol process, a process that uses biomass and natural gas as feedstocks to maximize methanol yields and minimize greenhouse gas emissions. EPA's APPCD has established a laboratory in which to conduct experiments on the critical reactions involved in the Hynol process. In this study, an integral fixed-bed reactor was used to perform kinetic measurements for methane-steam reforming at simulated Hynol operating conditions. The activity of a commercially available Ni-catalyst was evaluated. A kinetic model was developed for quantitatively interpreting the experimental data. The intrinsic reaction rates at different temperatures were measured using crushed catalyst pellets, resulting in an activation energy of 28 kcal/mol. The effectiveness factor for the commercial catalyst pellets (16 mm in diameter and 10 mm long) was determined and correlated as a function of reaction temperature. Experimental results indicate that a steam-to-carbon ration of 2.5 is appropriate. The carbon monoxide and carbon dioxide in the feed gas were found to be insensitive to the catalyst performance within the range of the experimental study. The hydrogen in the feed gas helps catalysts remain in the reducing state and prevents carbon deposition.

17.		KEY WORDS AND DOCUMENT ANALYSIS		
a. DESCRIPTORS		b. IDENTIFIERS/OPEN ENDED TERMS	c. COSATI Field/Group	
Pollution	Natural Gas	Pollution Control	13B	21D
Catalysis	Methane	Stationary Sources	07D	
Nickel	Steam	Hynol Process	07B	
Carbinols		Methanol	07C	
Greenhouse Effect			04A	
Biomass			08A, 06C	

18. DISTRIBUTION STATEMENT	19. SECURITY CLASS *(This Report)*	21. NO. OF PAGES
Release to Public	Unclassified	90
	20. SECURITY CLASS *(This page)* Unclassified	22. PRICE

ABSTRACT

The Hynol process, which uses biomass and natural gas as feedstocks to maximize

methanol yields and minimize greenhouse gas emissions, is under evaluation by APPCD of EPA.

A laboratory has been established to conduct experiments on the critical reactions involved in the

Hynol process. In this study, an integral fixed-bed reactor was used to perform kinetic

measurements for methane-steam reforming at simulated Hynol operating conditions. The

activity of a commercially available Ni-catalyst was evaluated. A kinetic model was developed

for quantitatively interpreting the experimental data. The intrinsic reaction rates at different

temperatures were measured using catalyst powders smaller than 0.1 mm, resulting in an

activation energy of 28 kcal/mol. The effectiveness factor for the commercial catalyst pellets

(16 mm in diameter and 10 mm long) was determined and correlated as a function of reaction

temperature. Experimental results indicate that a steam-to-carbon ratio of 2.5 is appropriate. The

carbon monoxide and carbon dioxide in the feed gas were found to be insensitive to the catalyst

performance within the range of the experimental study. The hydrogen in the feed gas helps

catalysts remain in the reducing state and prevents carbon deposition. The experimental results

showed that the catalyst activity dropped when the hydrogen partial pressure in the feed gas was

below a certain value. The size of a steam reformer suitable for the Hynol demonstration plant

was estimated. The study concludes that the commercial Ni-catalyst can be used for the

methane-steam pyrolysis of the Hynol process.

TABLE OF CONTENTS

LIST OF TABLES

LIST OF FIGURES

NOTICE

ACKNOWLEDGMENTS

METRIC CONVERSION FACTORS

Readers more familiar with the metric system may use the following factors to convert the non-metric units used in this report:

1 in	=	2.54 cm
1 ft	=	30.48 cm
1 lb	=	0.454 kg
1 psi	=	6.89 kPa
1 atm	=	101.3 kPa

SECTION 1.0

INTRODUCTION

Concerns regarding air quality, global climate change, and the national energy security

impacts of the intensive uses of gasoline in the transportation sector have raised interest in

alternative and renewable fuels.

Methanol has potential as an alternative fuel. It is a chemically simple liquid fuel,

compatible with the existing automotive refueling infrastructure. It can be made from a variety

of domestic feedstocks and is relatively inexpensive to produce. The combustion of methanol in

internal-combustion engines is very efficient and produces fewer toxic emissions than gasoline

(Motor Vehicle Emission Laboratory, 1989). In addition, methanol is the most viable onboard

hydrogen source for fuel cells, which are being considered as a replacement for internal-

combustion engines for road transportation. Fuel cells are more efficient than internal

combustion engines and produce no pollutants.

About 75 percent of commercial methanol production uses natural gas as feedstock. The

process includes steam reforming, methanol synthesis, and purification. Steam reforming

converts natural gas into the synthesis gas, a mixture of hydrogen and carbon monoxide, which is

then synthesized to methanol. Although steam reforming is conducted at 15 to 20 atm and 800 to

900°C, methanol synthesis operates at 50 atm and 260°C. Both reactions require catalysts to

achieve high methane conversion and methanol yields. The overall reaction is expressed as:

1

$$CH_4 + H_2O \rightarrow CH_3OH + H_2 \tag{I}$$
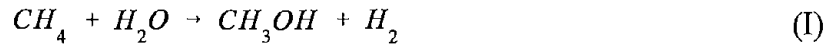
As shown in Equation I, steam reforming produces excess hydrogen for methanol production, which is usually used as combustion fuel.

Synthesis gas can also be produced by the steam gasification of coal or biomass. Because the amount of CO_2 absorbed by photosynthesis during the growth of biomass is equal to the amount released when it is finally used, the use of biomass as feedstock for methanol production offers advantages in reducing greenhouse gas emissions. However, biomass contains insufficient hydrogen, and the H_2/CO ratio in the synthesis gas produced by biomass steam gasification is not suitable for methanol synthesis. An additional step, water-gas shift reaction, is usually needed. In the shift converter, part of the CO in the reforming product is further reacted with steam to produce more H_2. The excess CO_2 formed is removed before methanol synthesis. If $CH_{0.4}O_{0.6}$ is used to represent a typical biomass composition, the overall reaction for this process is:

$$CH_{1.4}O_{0.6}\ (biomass) + 0.7H_2O \rightarrow 0.7CH_3OH + 0.3CO_2 \tag{II}$$
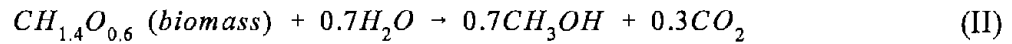
Steam gasification is highly endothermic. The energy required for steam gasification is provided by burning a portion of biomass with oxygen within the gasifier. The requirements for CO shifting, CO_2 removal, and oxygen supply increase capital and operation costs. As a result, methanol production from biomass has not been cost effective.

2

The idea of using the excess hydrogen from natural gas steam reforming to gasify biomass for methanol production has led to the invention of a new process: the Hynol process (Steinberg and Dong, 1994). The Hynol process maximizes methanol yields by using biomass and natural gas as co-feedstocks and combining biomass gasification and natural gas reforming as consecutive steps, as illustrated by the following overall reaction:

$$CH_{1.4}O_{0.6} + 0.9CH_4 + 1.3H_2O \rightarrow 1.9CH_3OH \tag{III}$$
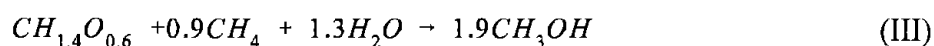
The process consists of three reaction steps: (1) gasification of biomass at 30 atm and 800°C with the H_2-rich gas recycled from methanol synthesis, (2) steam reforming of the product gas with an addition of natural gas feedstock at 25 atm and 950 to 1000°C, and (3) methanol synthesis of the produced H_2 and CO at 30 to 50 atm and 260°C. The process flowsheet is presented in Figure 1. Because biomass is gasified by the gas recycled from the methanol synthesis step, which is enriched with the excess hydrogen, the overall yield of methanol from biomass is increased. CO shifting and CO_2 removal, required for the steam gasification process, are no longer necessary. The exothermic reaction of biomass with hydrogen eliminates the need for expensive O_2 plants or complicated external heating systems for gasification. The integrated configuration, which uses the heat recovered from steam reforming to preheat the gasification feed gas and generate steam for methane reforming, increases process thermal efficiency.

The Air Pollution Prevention and Control Division (APPCD) of the National Risk Management Research Laboratory, U.S. Environmental Protection Agency (EPA), has conducted

3

a theoretical evaluation of process options for the production of transportation fuel from biomass and has concluded that the Hynol process represents a promising technology for maximizing fuel production with minimum greenhouse gas emissions (Borgwardt, 1995). Consequently, the APPCD established a laboratory to further assess the process feasibility and to carry out fundamental studies on the reactions that are crucial to the Hynol process. These studies are intended to provide preliminary answers to questions regarding biomass gasification kinetics at specific operating conditions of Hynol process and the conditions necessary for steam reforming the gasification products, and to provide quantitative information to support the design and operation of a bench-scale demonstration plant.

The study of biomass gasification under the Hynol process conditions was conducted using a thermobalance reactor (TBR). The TBR testing studied the effects of biomass particle size, residence time, reaction temperature, and feed gas composition on biomass gasification rates. The kinetic model developed for the interpretation of experimental data was able to predict gasification rates and biomass conversion at different operating conditions. The results of that study have been published (Dong and Cole, 1996; Dong and Borgwardt, 1996).

The steam reforming reaction of the Hynol process is addressed in this report. Using a fixed-bed reactor, the intrinsic reaction rates and the effectiveness factor for a commercially available nickel catalyst were evaluated. The minimum steam-to-carbon ratio required to prevent the carbon deposition on catalysts was determined for Hynol process conditions. The study also investigated the effects of reaction temperature and feed gas composition on methane conversion and reaction rates. This report summarizes these experimental results.

SECTION 2.0

PREVIOUS KINETIC STUDIES

In conventional steam reforming, natural gas feedstock is desulfurized (usually to less than 0.5 ppm H_2S), mixed with steam, and preheated to between 425 and 550°C. This mixture is fed to a reactor where it passes through an arrangement of externally fired tubes containing a nickel catalyst. The process usually operates at 15 to 20 atm and 800 to 900°C. The space velocities are on the order of 5000 to 8000 h^{-1}. Steam-to-carbon ratios range from 2.5 to 3.5. In a well-designed reformer, up to 95 percent of the methane is converted; the product gas usually attains a composition-representative equilibrium concentration at a temperature 10 to 15°C below the actual exit temperature of the catalyst bed. Nickel is the most widely used catalyst for steam reforming. Because the activity of a catalyst is closely related to the available surface area, nickel metal is usually dispersed on an alumina support to maximize the stable nickel surface area available to the reactants.

The reaction of methane with steam is complex. Various reaction mechanisms have been proposed. The commonly accepted mechanism for steam reforming is Reaction (IV) followed by Reaction (V):

$$CH_4 + H_2O \rightleftharpoons CO + 3H_2 \qquad \text{(IV)}$$

$$CO + H_2O \rightleftharpoons CO_2 + H_2 \qquad\qquad\qquad\qquad (V)$$

Akers and Camp (1955) were probably the first researchers to conduct a kinetic study for steam reforming using a nickel catalyst supported on diatomite. The catalyst pellets were 3.18 mm cylinders. The experimental results obtained at one atm and from 340 to 640°C showed a first-order reaction mechanism. The rate of reaction over the whole range of conversion is directly proportional to the partial pressure of methane,

$$r = \frac{dN_{CH_4}}{dt} = k\, p_{CH_4} \qquad\qquad\qquad\qquad (1)$$

where r = reaction rates, mol/h-g of catalyst. There was no dependence on other reactants. The reaction rate constant, k, was reported to be represented by an Arrhenius expression:

$$k = k_o \exp\left(-\frac{E_A}{RT}\right) \qquad\qquad\qquad\qquad (2)$$

where the pre-exponential factor, k_o = 127 mol/g-h-atm; the activation energy, E_A = 8,778 cal/mol; the gas law constant, R = 1.987 cal/mol-K; and the reaction temperature, T, is in K.

However, Bodrov et al. (see Agnelli et al., 1987) found that, at atmospheric pressure, a certain correlation exists between the partial pressures of CO, H_2, and H_2O. Their influence varies with temperature. At temperatures below 600°C, the reaction rates are inhibited by the presence of hydrogen:

For 400°C < T < 500°C

$$r = k \frac{p_{CH_4}}{p_{H_2}}$$
(3)

For 500°C < T < 600°C

$$r = k \frac{p_{CH_4}}{p_{H_2}^{0.5}}$$
(4)

At temperatures above 700°C, the rate is also influenced by the presence of CO in the feed gas.

For 700°C < T < 900°C

$$r = k \frac{p_{CH_4}}{1 + a \dfrac{p_{H_2O}}{p_{H_2}} + b \, p_{CO}}$$
(5)

An activation energy, E_A, of 19,400 cal/mol was obtained. The constants a and b were 0.5 and 2.0 atm^{-1} at 800°C, and 0.2 and 0 atm^{-1} at 900°C, respectively. Bodrov et al. concluded that

water-gas shift equilibrium was always established (Ridler and Twigg, 1989). However, Gerhard and Moe (1965) found that it was not at equilibrium.

Allen et al. (1975) measured the methane conversion at 640°C and pressures up to 18 atm over a Ni-catalyst and correlated it to a time factor (g cat-hr/mol) using a third-degree polynomial. They proposed a reaction mechanism and concluded that the desorptions of CO and CO_2 were controlling steps for steam reforming.

Munster and Grabke (1981) proposed that methane-steam reforming involved methane decomposition followed by a reaction of adsorbed carbon with steam. The overall reaction was controlled by the first reaction. Therefore, Equation (1) can be used to express the steam reforming reaction rate over nickel catalysts. However, Munster and Grabke obtained an activation energy of 38,000 cal/mol.

Agnelli et al. (1987) studied the dependence of the conversion of the methane-steam reforming reaction on the partial pressures of methane, hydrogen, and water. They found that the reaction is first order with respect to methane partial pressure, and that the influence of the reactants and products (except methane) is small enough to allow the use of a first-order kinetic equation. An activation energy of 41,650 cal/mol was reported. By comparing the ratios of the pressures of products to reactants for both Reaction (IV) and Reaction (V), they concluded that Reaction (V) was close to equilibrium.

Xu and Froment (1989) measured the intrinsic reaction rates of steam reforming at temperatures up to 575°C and pressures up to 15 atm. Their experimental results showed that there were no significant internal diffusion limitations for catalysts sized from 0.17 to 0.25 mm.

An activation energy of 57,000 cal/mol was reported. They proposed a more general kinetic model, which assumed a triangular reaction scheme in methane, carbon monoxide, and carbon dioxide. Xu and Froment claimed that Reaction (V) was always close to equilibrium at 10 to 15 atm but not at three to five atm.

Some of the reported activation energy data for steam reforming are compared in Table 1. It can be seen that the data are scattered. By reviewing a number of kinetic studies, Ridler and Twigg (1989) pointed out that the lack of appreciation of diffusion and heat transfer limitations is the primary reason for discrepancy in the kinetic results. They compared the results of methane steam reforming, methane cracking and its exchange with deuterium over nickel films and found that, in each case, the activation energy (in the absence of different effects) is about 31 kcal/mol.

A literature survey was performed for kinetic studies of steam reforming (Dong, 1994). The resulting report reviewed the various mechanisms and kinetics of steam reforming reaction, and carbon deposition on catalysts, as well as possible uses of noble metal catalysts.

Previous studies have been limited mostly to relatively lower pressures and temperatures. Small sizes of catalysts were used. In the Hynol process, however, steam reforming operates at 25 to 30 atm and 950 to 1000°C, conditions that are beyond the range of the previous studies. The feed gas into steam reformers is also different: a mixture of gasification product gas with an addition of natural gas feedstock, which contains 15 to 30 percent hydrogen as well as some CO and CO_2. No prior measurements have been reported under such Hynol-specific operating conditions. This study provides this important information for the Hynol process evaluation and development.

SECTION 3.0

EXPERIMENTAL

3.1   Experimental Apparatus

Figure 2 is a schematic diagram of the fixed-bed reactor used in this study. The reactor

design was based on a double-shell, balanced pressure system, which allows for high pressure

and high temperature operation. The reactor consists of a 2.09 cm inside-diameter reactor tube

and a 30.5-cm diameter stainless-steel, pressure-retaining vessel. The reactor tube was made of

310 stainless steel and was electrically polished to remove the nickel contained on the wall

surface of the reactor tube. The reactor was 120 cm long.

In the pressure-retaining vessel, a separately controlled, three-zone electrical heater

surrounded the reactor tube. Both the top and middle heater zones were 1.4 kW and 30.5 cm

long. The bottom heater zone was 0.7 kW and 15.2 cm long. The top heater zone served for

preheating the feed gas. The reaction temperature was controlled by the other two heating

elements.

The annular volume between the heater and the vessel body was densely filled with

Inswool® bulk insulation fibers to minimize heat loss. During testing, a constant nitrogen flow

of 0.1 SLPM entered the pressure-retaining vessel. It then joined with the process gas exiting

from the condenser to balance pressures between the reactor tube and the pressure-retaining

vessel. At 800°C and a gas flow rate of 10 SLPM in the reactor, the measured reactor pressure was 25.17 atm when the vessel pressure was held at 25.07 atm, indicating a 0.1 atm of pressure difference.

A perforated-plate catalyst support was used to position catalysts in the middle section of the reactor. Catalysts were charged into the reactor through the top plate flange. For those tests with a single commercially sized catalyst pellet, 45 ml and 65 ml of 3mm-diameter ceramic Raschig rings were packed under and above the pellet to ensure a uniform gas flow through the reactor. When crushed catalyst powders were used to measure the intrinsic reaction rates, the Raschig rings served as a diluent mixed with the catalyst powders to improve the distribution of heat load in the reactor.

Three K-type thermocouples were inserted from the bottom of the reactor through separate 1/8-in stainless-steel tubing lances to measure the temperatures at the top, middle, and bottom of the catalyst bed.

The flowsheet of the experimental equipment used in this study is shown in Figure 3. The feed gas components -- methane, hydrogen, and carbon monoxide -- were supplied from individual gas cylinders. The carbon dioxide was obtained from a custom-blended CO_2/H_2 cylinder containing 30 percent carbon dioxide. The purity of each gas component is presented in Table 2. The flow rates of these gas components were controlled separately by the mass flow controllers, and then were blended in an on-line gas mixer to simulate the Hynol steam pyrolysis conditions.

A constant steam flow for the reforming reaction was generated by an electrically heated steam generator in which distilled water was injected through an HPLC metering pump and then vaporized and mixed with the other feed gases. The steam generator was a 4.4-kW split tube furnace-type heater with a 18-in long, 3-3/4 I.D. heated chamber. A 20-ft long, 25-turn coil of 1/4-in stainless steel tube was horizontally mounted in the heater to provide sufficient heat transfer surface area for steam generation. The steam generator was controlled at 380°C.

The gas mixture from the steam generator was preheated to 400°C by the on-line heating tapes and then was entered into the top of the reactor. In the top reactor heater zone, the gas mixture was further heated to the required reaction temperature before contacting catalysts.

The product gas exiting the bottom of the reactor was cooled in a 52-in long vertical water-cooled condenser followed by an ice-bath to remove moisture. Upon exiting the ice bath, the gas temperature was well below 15°C. The water condensate collected in the 0.5-liter trap was weighed every 30 minutes during testing to determine the moisture in the product gas.

The offgas, from which moisture has been removed by the condenser, was then depressurized through a back-pressure regulator and vented to atmosphere. The offgas flow rate was measured by an on-line dry gas meter.

The offgas composition was analyzed by a Hewlett Packard 5890 Series II gas chromatograph (GC) equipped with a 30-ft-long HayeSep DB column and a thermal conductivity detector (TCD). An automatic sampling valve, controlled by the integrator keyboard, took gas samples every 30 minutes from the sampling port and injected them into the heated GC injection port. A gas purifier, filled with sodium/calcium sulfate, was placed between the sampling port

and the automatic valve to further remove moisture and impurities from gas samples. Helium was used as a carrier gas to sweep samples into the column. The column separated the samples into the following compounds: hydrogen, nitrogen, carbon monoxide, methane, and carbon dioxide, which were detected by the TCD and recorded as peaks on the integrator. The integrator calculated the composition of each compound based on its peak area and relative response factor. Table 3 summarizes the operating conditions set for GC and integrator. A typical printout from the GC integrator is shown in Figure 4.

Pressure and temperature measurement locations are shown in Figure 3.

A personal computer (PC) controlled the system. LabTech control software was used to display, control, and record the pressure, temperatures, and flow rates. The data were logged every 30 minutes into a set of specially designed Excel spreadsheets, which provided automatic calculations for steam feed rates, water condensate rates, offgas flow rates, methane conversion, as well as material balance checking. An example of the recorded data spreadsheets is provided in Figure 5.

3.2   Experimental Procedures

An activation process is usually required when fresh catalysts are used. The purposes of activation are to stabilize supported metal crystals and remove adventitious poison. The techniques used for catalyst activation depend primarily on the nature of the catalyst, but also on the process for which the catalyst is to be used. For Ni-catalyst used in methane-steam reforming, Agnelli et al. (1987) suggested reducing catalysts by a 10 percent gaseous mixture of H_2 and N_2 at reaction temperature for 15 hours. In this study, a commercially recommended

13

activation procedure for Ni-catalyst was employed (Ridler and Twigg, 1989). The procedure involved passing a reducing gas containing an 8:1 ratio of steam to hydrogen through the catalyst at 800°C for six hours. The hydrogen feed rate was set to 1.2 SLPM in all the activation runs.

To start a test run, catalysts with known weights were first loaded into the reactor. The system was pressurized with 10 SLPM of nitrogen through the catalyst bed and one SLPM of balance nitrogen through the pressure-retaining vessel. After the system reached the desired operating pressure, a SNOOP liquid leak detector was used to check for leaks. The reactor was then heated up at a rate less than 200°C/h.

When the desired reaction temperature was reached, the balance nitrogen flow in the pressure-retaining vessel was reduced to 0.1 SLPM. The gas flow in the catalyst bed was switched from nitrogen to the feed gas mixture. The heater elements were carefully controlled to maintain a consistent temperature at the top, middle, and bottom of the catalyst bed. After stabilization, the experimental data were recorded at 30-minute intervals.

When the run was complete, the reactor was cooled down at a rate less than 200°C/h. The system was then depressurized. Careful control of heating and cooling rates prevented thermal damage to the heating elements and catalyst pellets.

3.3   Catalyst Properties

The commercial Ni-based catalyst used in this study was 16 mm in diameter and 10 mm long. It was ring shaped with seven 3-mm diameter holes. The catalyst contained 15 percent nickel, 25 percent magnesium oxide, and 60 percent aluminum oxide. Its melting point was 1400°C.

The sphericity, ϕ_S, of the catalyst pellet was estimated based on the above given

geometric dimensions in the following equation:

$$\phi_S = (\frac{surface \ of \ sphere}{surface \ of \ particle})_{both \ of \ same \ volume} = \frac{622.9 \ mm^2}{1586.8 \ mm^2} = 0.39 \qquad (6)$$

An average particle density of 1.75 g/cm³ for this type of catalyst pellet was determined

from the weight and volume measurements, as summarized in Table 4. The solid density was

estimated to be 4.65 g/cm³ based on the catalyst ingredients and illustrated in Table 5. The

porosity of the catalyst was then estimated as:

$$\varepsilon = 1 - \frac{\rho_P}{\rho_S} = 1 - \frac{1.75}{4.65} = 0.62 \qquad (7)$$

where ε = porosity
      ρ_P = particle density, g/cm³
      ρ_S = solid density, g/cm³

The specific surface area and average pore size of the catalysts were measured with a

Micromeritics Surface Area Analyzer and calculated using the Brunauer-Emmett-Teller (BET)

method. The results for the fresh catalyst and the catalyst after 20 hours of operation at 25 atm

and 1000°C are provided in Table 6.

15

Table 7 compares the catalyst properties in this study with those reported in the previous publications.

3.4   Feed Gas Composition and Flow Rates

The feed gas composition used for the base case studies was chosen to simulate the results of the Hynol process simulation, which were obtained using ASPEN PLUS as shown in Figure 6 (Borgwardt, 1994). In this report, the Hynol feed gas always refers to the feed gas mixture with the following mole ratios of components:

$$\frac{CO}{CH_4} = 0.266; \quad \frac{CO_2}{CH_4} = 0.12; \quad \frac{H_2}{CH_4} = 1.06$$

The steam-to-carbon ratio in the feed gas was a parameter to be investigated. The nitrogen in the feed gas was neglected in the study because of its inert nature and the small quantity involved.

The total feed-gas flow rate in the base case study was determined based on the following considerations: (1) The gas velocity in the reactor under the reaction conditions should be high enough to minimize the resistance to the gas-film mass transfer; (2) the maximum capacity of the water-cooling condenser was 50 mL/min; (3) the maximum capacity of the trap for condensate collection was 0.4 liters in 30 minutes or a rate of 13 mL/min; and (4) the methane feed rate should be less than 5.6 SLPM to allow a single methane cylinder to supply methane for at least

16

16 hours. As a result, the rates of feed gas components in the base case were set to $CH_4 = 3.0$ SLPM, $H_2 = 3.181$ SLPM, $CO = 0.799$ SLPM, and $CO_2 = 0.359$ SLPM.

An operating pressure of 25 atm was chosen for all the experimental runs based on the consideration of a designated pressure of 30 atm for biomass gasification and an estimated pressure drop of 5 atm from the exit of the gasifier to the exit of the steam reformer in the Hynol process.

SECTION 4.0

KINETIC MODEL

Most investigators of methane-steam reforming have agreed on a kinetics of first order with respect to the partial pressure of methane. A constant gas flow throughout the catalyst bed was assumed when they integrated the first order reaction rate expression to obtain the reaction rate constants. The steam feed in the reforming reaction is usually in excess of that required to suppress carbon formation on catalysts and improve reaction yields. Therefore, the first-order scheme with respect to the methane partial pressure is considered appropriate and is adopted in the kinetic model for the Hynol steam pyrolysis reaction. However, the assumption of constant gas flow is valid only if a small amount of methane converted across the catalyst bed. As Reaction (IV) shows, each mole of methane reacting with one mole of steam produces one mole of carbon monoxide and three moles of hydrogen, resulting in two moles of net increase in the total gas flow. In other words, the total mole flow rate increases as the process gas passes through the catalyst bed. This increase in total gas flow rate can be significant if the conversion is high. For this reason, the increase in total flow rate due to reaction was taken into account in developing a quantitative kinetic model of the Hynol steam reforming reaction suitable for an engineering application.

18

If the reaction rate, r, is defined as the moles of methane converted by one gram of catalyst per hour, the first order reaction rate can be expressed by:

$$r = -\frac{dF_{CH4}}{dW} = k\,P_{CH4} = k\,\frac{F_{CH4}}{F_T}\,P \qquad (8)$$

where F_{CH4} = methane flow rate, mol/h
k = rate constant for Reaction (IV), mol/g-h-atm
P = reactor pressure, atm
P_{CH4} = methane partial pressure, atm
W = catalyst weight, g
F_T = total process gas rate, mol/h

It is convenient to express the reaction rate in terms of methane conversion. The methane conversion is a measure of how far the steam reforming reaction has progressed and is defined as the methane reacted divided by the methane fed to the reactor:

$$X_{CH4} = \frac{F_{CH4}^0 - F_{CH4}}{F_{CH4}^0} \qquad (9)$$

where F^0_{CH4} = methane mole feed rate, mol/h
F_{CH4} = methane rate after reaction, mol/h

In the experiments, F_{CH4} at the exit of the reactor can be calculated from the offgas flow rate measured by the dry gas meter and the methane mole fraction in the offgas obtained from the GC analysis.

Because the total gas flow rate, F_T, in Equation (8) increases as the reaction proceeds, it should be a function of X_{CH4}. From the stoichiometric relationship of Reaction (IV) and Equation (9), the following equation can be obtained:

$$F_T = F_T^0 + 2F_{CH4}^0 X_{CH4} \qquad (10)$$

where $F_T^0 =$ initial total feed rate, mol/hr
$F_{CH4}^0 =$ initial methane feed rate, mol/hr

Substituting Equations (9) and (10) into Equation (8) results in a reaction rate expression in terms of methane conversion as:

$$\frac{dX_{CH4}}{dW} = k\,P\,\frac{1 - X_{CH4}}{F_T^0 + 2\,F_{CH4}^0\,X_{CH4}} \qquad (11)$$

Because the methane conversion is zero at the reactor inlet, the initial condition is:

$$at \quad W = 0 \qquad X_{CH4} = 0 \qquad (12)$$

20

Integrating Equation (11) with the initial condition gives the methane conversion, X_{CH4}, as a

function of catalyst weight, W, by

$$X_{CH4} = -\ln(1 - X_{CH4}) \frac{F_T^0 + 2\ F_{CH4}^0}{2\ F_{CH4}^0} - \frac{k\ P\ W}{2\ F_{CH4}^0} \tag{13}$$

The above implicit equation must be solved iteratively. If the reaction rate constant is known,

the methane conversion for a given amount of catalyst can be calculated from Equation (13).

The equation can be rearranged to allow for the determination of the reaction rate constants from

methane conversion measurements:

$$k = \frac{1}{P\ W} [\ -2\ F_{CH4}^0\ X_{CH4} - (F_T^0 + 2\ F_{CH4}^0)\ \ln(1 - X_{CH4})\ ] \tag{14}$$

Because the catalyst weight, system pressure, and total and methane feed rates are known, the

rate constant can be calculated from the methane conversion observed from the experiment.

The primary focus of this kinetic study was methane conversion over catalysts because

the water-gas shift reaction is faster than the methane-steam reaction and is close to equilibrium

at high pressures and temperatures. The overall rate of methane-steam reforming is therefore

considered to be controlled by Reaction (IV).

21

SECTION 5.0

RESULTS AND DISCUSSIONS

A number of test runs have been made under the conditions of the steam reforming step of the Hynol process. Table 8 summarizes all the data obtained in those runs and addresses all of the variables considered potentially influential in the conversion of methane over catalysts at Hynol conditions. The results from these investigations are separately discussed in detail in the following sections.

5.1 Blank Tests

In order to ensure that the observed reaction results truly represented the catalyst performance, several blank tests were conducted to examine the catalytic effects of the reactor tube wall on the methane conversion. In the tests, methane and steam were introduced into an empty reactor. The feed gas was a mixture of 3.14 SLPM of methane and 5.13 SLPM of nitrogen. The steam-to-carbon ratio was 3.3. The reactor operated at 25 atm and 950°C. The typical experimental results are shown in Table 9. The difference between the methane flows into and out of the reactor averaged 0.64 percent, indicating that the methane conversion is negligible in the empty reactor tube.

5.2 Catalyst Stabilization

It is important that catalysts be stabilized before kinetic data can be collected. In an early kinetic study, Akers and Camp (1955) found that the activity of Ni-catalyst was constant; no change in the product gas composition was observed over a period of 6.5 hours. However, the deactivation of Ni-catalysts in the initial stage of use as a result of sintering was reported. The reported times for catalyst stabilization differ significantly, ranging from 70 hours (Xu and Froment, 1989) to less than 30 minutes (Rostrup-Nielsen, 1973). It is expected that the system operating conditions will affect the catalyst stabilization period. Higher pressures, temperatures, and steam-to-carbon ratios promote catalyst sintering and, thus, increase catalyst deactivation rates. The stabilization time must be determined experimentally.

A test was conducted to examine the stabilization time of the catalyst used in this study. The test was performed at 25 atm and 1000°C with 0.8 g of crushed Ni-catalyst powders. The Hynol feed gas composition was used. The steam-to-carbon ratio in the feed gas was 2.07. Methane conversion was measured every 30 minutes over the entire operation period of 27 hours. The observed variation in methane conversion with reaction time is presented in Figure 7. Under Hynol operating conditions, the activity of nickel catalysts decreased rapidly in the first five hours, after which a steady-state condition was reached. Thus, a minimum stabilization time of four to five hours is considered necessary before kinetic data collection can be started.

5.3 Minimum Steam Ratio

Carbon deposition on catalysts reduces the catalyst activity and, therefore, must be prevented. Carbon can be formed in the reactor in two basic ways. Carbon is formed in the

catalyst pores when the following two reactions are thermodynamically favorable for a given

mixture of CO, CO_2, H_2, CH_4 and H_2O

$$2\ CO\ =\ CO_2\ +\ C \tag{VI}$$

$$CO\ +\ H_2\ =\ H_2O\ +\ C \tag{VII}$$

Carbon can also be formed as a result of thermal cracking by:

$$CH_4\ =\ 2\ H_2\ +\ C \tag{VIII}$$

Carbon resulting from hydrocarbon cracking does not usually form in the inner pores of the

catalyst, but rather as soot-like deposits on the outside surface of the catalyst.

To avoid carbon formation, a high steam-to-carbon ratio in the feed gas must be

employed. The steam ratio in conventional steam reforming processes usually ranges from 2.5 to

3.5.

The feed gas contains hydrogen in the Hynol steam pyrolysis reaction. This hydrogen

assists in preventing carbon formation and in maintaining the catalyst in a reducing state. A

relatively lower steam ratio requirement is thus possible for the Hynol process. Tests were

conducted to estimate the appropriate steam ratio under the Hynol operating conditions. The

tests operated at 25 atm and 950°C with two g of Ni-catalyst powders. Methane conversion was

continuously measured at a steam ratio of 1.5 for 30 hours. No methane conversion loss was

24

observed during the test, but carbon deposition was found at the exit of the reactor. When the steam ratio was greater than two, carbon formation was found to be eliminated. Therefore, the minimum steam ratio is considered to be two at the test conditions.

The independence of the reaction rate upon the steam ratio above the minimum can be illustrated by comparing the experimental results obtained at different steam ratios for a single commercially sized catalyst pellet, as shown in Figure 8. It was noted from the figure that, at the same reaction temperature, the reaction rate is zero order with respect to the steam ratio. Thus, a steam ratio considerably higher than the minimum is undesirable because a higher steam ratio requires more heat load. The appropriate range of steam ratios for the Hynol steam pyrolysis is considered to be from 2 to 2.5.

5.4   Intrinsic Reaction Rate

Gaseous chemical reactions over a solid catalyst system involve mechanistic steps such as external mass transfer, pore diffusion, chemisorption, and intrinsic reaction. The overall reaction rate is controlled by the slowest mechanistic step. The intrinsic kinetics means that the measured rate is free from pore diffusional influence or any other mass transfer influence. Therefore, the intrinsic reaction rate must be measured under conditions showing negligible restrictions for mass transfer and pore diffusion.

Pore diffusion resistance can be minimized by reducing catalyst size. Agnelli et al. (1987) indicated that catalyst pellets should be crushed down to a maximum size between 0.30 and 0.42 mm to avoid internal diffusion effects. Xu and Froment (1989) suggested this critical catalyst size should be between 0.17 and 0.25 mm. In this study, intrinsic kinetics was measured

25

using powders smaller than 0.1 mm, crushed from commercial catalyst pellets. To ensure representativeness, about 500 grams of catalyst pellets was ground and screened to obtain testing samples.

The intrinsic reaction rates were measured at reaction temperatures ranging from 900 to 1000°C. Two series of runs were conducted. In each test, a one-gram sample of Ni-catalyst powders was charged into the reactor in which ceramic rings act as diluents to improve heat distribution. The Hynol feed gas composition then was simulated. The system pressure was kept at 25 atm. The methane conversions observed at different temperatures were plotted as a function of reaction temperature as shown in Figure 9. The plot displays a close agreement between the conversion results obtained from the two samples of catalyst powders, indicating a good repeatability of the measurements. The results also showed that methane conversion in steam reforming increases with reaction temperature. The reaction rate constants at different reaction temperatures were calculated from the conversion data using the kinetic model, Equation (14), and are summarized in Table 10. The activation energy was then determined by Arrhenius law. The reaction rate constants were plotted against the reciprocal of the absolute temperature in Figure 10. The pre-exponential factor, k_o, and the activation energy, E_A, thus obtained were 65,552 mol/g-h-atm and 27.97 kcal/mol. The activation energy is close to the previously reported 31 kcal/mol measured in the absence of diffusion effects (Ridler and Twigg, 1989).

The influence of the external gas film resistance on the intrinsic kinetics under the actual experimental conditions was theoretically evaluated. The rate of methane transport from the bulk gas phase to the catalyst external surface was calculated by:

$$N_{CH4} = k_g A_P (P_{CH4,g} - P_{CH4,e})\qquad(15)$$

where N_{CH4} = moles of methane transferred from gas to solid, mole/s
   A_P = catalyst external surface, cm^2
   k_g = mass transfer coefficient between gas and solid, mol/s-cm^2-atm
   $P_{CH4,g}$ = methane partial pressure in the bulk phase, atm
   $P_{CH4,e}$ = methane partial pressure at the catalyst external surface, atm

in which the mass transfer coefficient, k_g, was estimated by the following correlations for a

packed catalyst bed at Re <190 (Froment and Bischoff, 1979):

$$1.66\ Re^{-0.51} = \frac{k_g P A_T}{F_T}\ Sc^{2/3}\qquad(16)$$

with

$$Re = \frac{U\ dp\ \rho_m}{\mu_m}\qquad(17)$$

$$Sc = \frac{\mu_m}{\rho_m D_m}\qquad(18)$$

$$A_T = \frac{\pi}{4} \times D_T^2\qquad(19)$$

27

where Sc =   Schmidt dimensionless number
       Re =   Reynolds dimensionless number
       F_T =   Total gas mole flow, mol/s
       P =   System pressure, atm
       μ_m =   viscosity of gas mixture, g/cm-s
       ρ_m =   density of gas mixture, g/cm^3
       D_m =   diffusivity of methane through the gas mixture, cm^2/s
       U =   gas velocity, cm/s
       dp =   catalyst diameter, cm
       A_T =   cross-sectional area of the reactor, cm^2
       D_T =   diameter of the reactor, cm

The transport properties of the feed gas mixture were calculated from individual gas properties

using the methods discussed by Froment and Bischoff (1979) as follows:

The density of each pure gas component, ρ_i, under the reaction conditions was calculated

by:

$$\rho_i = \frac{M_i}{22.4} \times \frac{273 \times P}{(T+273) \times 1} \tag{20}$$

where M_i =   molecular weight of individual gas component, g/mol
       T =   reaction temperature, °C.

The density of the gas mixture under the reaction conditions was then calculated by the following

equation:

$$\rho_m = \sum_i \rho_i \frac{P_i}{P_T} \tag{21}$$

where P_i = partial pressure of individual gas component, atm.

28

To calculate the viscosity of the gas mixture, the viscosities of pure gases at the critical

conditions, $\mu_{C,i}$, were first estimated by Equation (22) (Bird et al., 1960):

$$\mu_{c,i} = 7.7 M_i^{1/2} P_{c,i}^{2/3} T_{c,i}^{-1/6}$$ (22)

where $P_{c,i}$ and $T_{c,i}$ are critical pressure and temperature of the i-th gas component. The viscosities

of the pure gases under the operating conditions were then calculated from:

$$\mu = \mu_c \, \mu_r$$ (23)

where μ_r was obtained as a function of $P_r = P/P_c$ and $T_r = T/T_c$ (Bird et al., 1960). The viscosity

of the gas mixture was then obtained by:

$$\mu_{mix} = \sum_{i=1}^{n} \frac{P_i \mu_i}{\sum_{j=1}^{n} P_j \Phi_{ij}}$$ (24)

in which

$$\Phi_{ij} = \frac{1}{\sqrt{8}} \left(1 + \frac{\mu_i}{\mu_j}\right)^{-1/2} \left[1 + \left(\frac{\mu_i}{\mu_j}\right)^{1/2} \left(\frac{M_j}{M_i}\right)^{1/4}\right]^2$$ (25)

The diffusivities of methane in other gas components at low pressure were calculated based on

Equation (26) (Bird et al., 1960):

$$D_{CH4-i} = a\left(\frac{T}{\sqrt{T_{c,CH4}T_{c,i}}}\right)^b (P_{c,CH4}P_{c,i})^{1/3}(T_{c,CH4}T_{c,i})^{5/12}\left(\frac{1}{M_{CH4}}+\frac{1}{M_i}\right)^{1/2} \qquad (26)$$

in which the constants a and b were given as:

for nonpolar gas-pairs,

$$a = 2.745 \times 10^{-4} \qquad \text{and} \qquad b = 1.823$$

for H_2O with a nonpolar gas,

$$a = 3.640 \times 10^{-4} \qquad \text{and} \qquad b = 2.334$$

The chart (Bird et al., 1960) was then used to correct the diffusivities to the operating conditions.

The diffusivity of methane through the gas mixture was calculated using the following equation

provided by Froment and Bischoff (1979):

$$D_m = \frac{P_T + 2P_{CH4}}{\frac{1}{D_{CH4-H2}}(P_{H2}+3P_{CH4}) + \frac{1}{D_{CH4-CO}}(P_{CO}+P_{CH4}) + \frac{1}{D_{CH4-CO2}}P_{CO2} + \frac{1}{D_{CH4-H2O}}(P_{H2O}-P_{CH4})} \qquad (27)$$

By substituting known data ($D_T = 2.667$ cm, P = 25 atm, T = 1000°C, $P_{CH4} = 4.79$ atm, $P_{H2} = 5.08$

atm, $P_{CO} = 1.27$ atm, $P_{CO2} = 0.57$ atm, and $P_{H2O} = 13.29$ atm) into the above equations, the

transport properties were calculated and are presented in Table 11.

From these estimated transport properties, the Schmidt number and Reynolds number were calculated to be 0.36 and 0.9. The film mass transfer coefficient, k_g, of 0.0001 mol/s-cm²-atm for 0.1 mm diameter catalysts was then obtained by Equation (16).

The methane transfer rate through the film of the catalyst was then calculated by Equation (15). If the mass transfer was a controlling step in this equation, the methane partial pressure at the catalyst surface was taken to be zero. The rate of methane transport to one gram of catalyst powders was

$$N_{CH4} = k_g A_P C_{CH4} = k_g \frac{6W}{dp \times \rho_P} P_{CH4} = 0.0001 \times \frac{6 \times 1}{0.01 \times 1.748} \times 4.79 = 0.164 \, mol/s \tag{28}$$

It was then compared with the initial intrinsic rate at 1000°C, which was calculated as

$$N_r = k_r \frac{F_{CH_4}}{F_T} PW = 0.000283 \times \frac{3}{15.67} \times 25 \times 1 = 0.00135 \, mol/s \tag{29}$$

It can be seen that, in this case, the overall reaction was limited by chemical reaction. Therefore, the measurements are considered to be representative of intrinsic kinetics.

5.5   Effective Activities of Commercial Catalyst Pellets

Although catalyst powders can minimize pore diffusion restriction and provide high catalytic activity, large pellets are always used in commercial reactors in order to reduce pressure drops across the catalyst bed. It is thus important to know the effective activity of the commercial-size catalyst pellets used in practical steam reformers. In this study, the overall

reaction rates over commercial Ni-catalyst pellets were measured. Two series of tests were carried out at 25 atm. One pellet of catalyst was charged for each series of tests, in which the methane conversion was measured at various temperatures ranging from 900 to 1000°C. The reaction rate constants obtained in the two series of tests increased with reaction temperature as shown in Figure 11. This figure shows a difference in the reaction rate constants obtained from the two catalyst pellets, indicating the possible existence of a variation in catalytic activity among the pellets. The figure also shows that catalyst pellets had substantially lower reaction rate constants than did powders, a result of the strong influence of pore diffusion within the large pellets. The importance of the pore diffusion in the overall reaction rate can be measured by the catalyst effectiveness factor (Froment and Bischoff, 1979), which is the ratio of the reaction rate observed with pellets to the intrinsic reaction rate as expressed by:

$$\eta_{eff} = \frac{(Observed\ reaction\ rate)}{(Intrinsic\ reaction\ rate)} = \frac{k_{obs}}{k} \tag{30}$$

The overall reaction rate of a catalyst pellet is thus equal to the intrinsic reaction rate multiplied by the effectiveness factor at the same operating conditons.

The effectiveness factors for the Ni-catalyst pellets used in this study were estimated from the experimental results of the pellets and the intrinsic kinetics discussed in Section 5.4. Considering the activity deviation among the tested catalyst pellets, a statistical analysis was conducted to calculate the effectiveness factors from observed reaction rate constants. The averaged effectiveness factors at different reaction temperatures were plotted with error bars in

32

Figure 12. The statistical analysis results were also summarized in Table 12. In the table, the maximum and minimum values of the effectiveness factor are obtained with a confidence interval of 95 percent. The results reflect a trend in which the catalyst effectiveness factor decreased as reaction temperature increased. The chemical reaction gets faster at a higher reaction temperature so that the restriction of pore diffusion becomes more dominant. The catalyst effectiveness factors for the Ni-catalyst pellets are well within the range of 0.01 to 0.3 for a similar commercial catalyst reported by Ridler and Twigg (1989). The effectiveness factor for the catalyst pellets used in this study was correlated with reaction temperature in the following expression:

for $900°C < T < 1000°C$

$$\eta_{eff} = 4.326 - 8.03 \times 10^{-3} T + 3.8 \times 10^{-6} T^2 \tag{31}$$

where T is in °C. If the weight of catalysts is known, the methane conversion at a specific reaction temperature can be calculated by

$$X_{CH4} = -\ln(1 - X_{CH4}) \frac{F_T^0 + 2 F_{CH4}^0}{2 F_{CH4}^0} - \frac{65552 \exp(\dfrac{-27970}{1.987 \, T}) \eta_{eff} \, P \, W}{2 F_{CH4}^0} \tag{32}$$

33

The calculation results of the above equation were compared with the experimental data as shown in Figure 13. Considering the difference in activity among the catalyst pellets used in the tests, the agreement between the prediction and observation is sufficiently good.

The mechanical strength of the commercial Ni-catalyst used was examined. A single 3.431-g catalyst pellet was loaded into the reactor. After 50 hours of testing under Hynol process operating conditions (25 atm and 1000°C), the catalyst pellet was discharged for physical examination. The pellet weighed 3.423 g after reaction and retained its original shape. No cracking or any other damage was observed, indicating that the catalyst is applicable to an operation temperature up to 1000°C. However, as mentioned previously, it is critical that the heating and cooling rate of the reactor be controlled below 200°C/h to prevent the damage of both catalyst and furnace caused by thermal shock.

5.6   Effects of Feed Gas Composition

In the Hynol process, the gas composition that is fed to a steam reformer occasionally may vary slightly. This variation is caused by a fluctuation in the composition of biomass and natural gas feedstocks or by the performance of the preceeding biomass gasifier. Thus, the sensitivity of catalyst activity to these potential fluctuations must be assessed. To do so, the dependence of the extent of methane conversion upon the partial pressures of carbon monoxide, carbon dioxide, and hydrogen in the feed gas was investigated.

The effects of the CO partial pressure in the feed gas were investigated by varying the CO feed rate while maintaining the other gas feed rates at the base study levels. The steam feed rate was fixed at 10.4 SLPM. Two series of runs (R036 and R038) were conducted with a single

pellet of Ni-catalyst. Test R036 was made at a temperature of 900°C and Test R038 was at 1000° C. In Test R038, the CO partial pressure in the feed gas was varied at four levels: 2.15, 1.13, 0.57, and zero atm, while the rates of other feed gases including steam were held constant. Two levels of the CO partial pressure, 0.73 and zero atm, were investigated In Test R036. The methane conversion was measured at these different CO pressure levels and was used to calculate the corresponding reaction rate constants. The results are presented in Figure 14 as a function of the CO partial pressure. It is noted that the reacton rate is nearly independent of the CO content of the feed gas as CO's partial pressure varies from zero to 2.2 atm. Therefore, it is concluded that the rate of the methane-steam reaction is unaffected by the CO content of the feed gas within the range of experimental conditions used in this study.

The effects on catalyst activity of the CO_2 in the feed gas were investigated at two reaction temperatures:1000°C and 900°C. At 1000°C, the reaction rate at the Hynol operating conditions was compared to the results achieved when the feed gas contained no CO_2. A zero-CO_2 condition was examined in two ways. In the first, steam was used as a make up gas to maintain the partial pressure constants of other gas components. In the second, nitrogen was used as a make-up gas. The reaction rate constants obtained under these two different CO_2 conditions, compared in Figure 15, show no significant change in catalyst activity when the CO_2 feed was cut off completely. In the tests at 900°C, the CO_2 feed rate was varied at three different levels of partial pressure: 0.96, 0.48, and zero atm. The results at 900°C shown in Figure 15 also indicated that the reaction rate is nearly constant as the CO_2 partial pressure increased from zero

to one atm. Therefore, it can be concluded that, as with carbon monoxide, changes in the CO_2 composition in the feed gas have no significant effects on catalyst activity.

The dependence of catalyst activity on the hydrogen in the feed gas is complicated. Three series of tests (R039, R041, and R042) were conducted by varying the hydrogen feed rate in different sequences at constant flow rates of the other feed gases to obtain the hydrogen partial pressure between 1.7 to 5.5 atm. All three tests showed a sharp drop in catalyst activity when the hydrogen partial pressure was below a certain level. Test R039 was made at 950°C. The change in methane conversion with the hydrogen partial pressure over time is plotted in Figure 16. The hydrogen partial pressure levels for each period of time are noted on the top of the conversion curve. It is evident that the deactivation occurs when the hydrogen partial pressure was reduced from 4.5 to 1.75 atm. In Test R041, the hydrogen feed rate varied periodically over this same broad range. As shown in Figure 17, the catalyst activity resumed when the hydrogen partial pressure was set back from a low level. No significant effects on catalyst activity were observed when the hydrogen partial pressure was above the critical level. In Test R042, the hydrogen feed rate was reduced from the Hynol condition to allow the reactor to operate at low hydrogen partial pressure for more than 10 hours. The results presented in Figure 18 show that the catalyst activity drops as the hydrogen feed rate is reduced but it cannot be recovered simply by resetting the hydrogen feed back to a high level, indicating the possible influence of the time period under low hydrogen partial pressures. The reason for substantial drop in methane conversion when increasing the hydrogen partial pressure from 1.91 to 5.81 atm is not clear and needs further investigation. The deactivation at a low hydrogen feed rate is caused by both carbon deposition

on catalyst surfaces and an insufficient reducing environment for nickel metal. The critical level of hydrogen partial pressure in the feed gas in the above experiments was around three to four atm, but is expected to be a function of other experimental variables. The limited results available in this type of investigation make a quantitative criterion difficult to determine.

Equation (13) indicates that the methane feed rate affects the methane conversion through both the time factor, W/F_{CH4}^0, and the initial methane composition in the feed gas, F_{CH4}^0/F_T. The increase in methane feed rate increases the methane partial pressure in the feed gas, resulting in an increased reaction rate, but a decrease in the residence time of the process gas in contact with catalysts. The methane conversion is thus an overall result of these two opposite effects. If Equation (14) holds true, the reaction rate constant calulated from the methane conversion results obtained from the test runs with different methane feed rates should be constant. Thus, two series of tests (R045 and R046) were conducted at various methane feed rates to verify the kinetic model developed in this study. The methane feed rate in the tests was varied from three to one SLPM, while the feed rates of the other gas components were kept constant. The reaction temperature in the tests was 950°C. The methane conversion was measured and used to calculate the reaction rate constants. The results in Figure 19 show that a constant k_{ob} is obtained in spite of the change in methane feed rate, indicating that the kinetic model is valid.

5.7 Demonstration Plant Sizing

The reaction rate of the Ni-catalyst pellets measured in this study can be used to determine the size of the steam reformer for the Hynol demonstration plant. The design

specification of the demonstration plant (Acurex Environmental, 1995) provides the following

data for the gas feed rates:

H_2 = 1860 mol/h; CO = 650 mol/h; CO_2 = 370 mol/h; CH_4 = 1960 mol/h

For H_2O/C = 2.5, the water feed rate is 7450 mol/h, and the initial total gas flow rate is 12290

mol/h. The reactor was assumed to operate at 25 atm and 950°C and reach 95 percent methane

conversion. The catalyst effectiveness factor at this condition is 0.117 from Equation (31). By

substituting all these data into Equation (32), the required catalyst weight was calculated as:

$$W = \frac{1}{65552\exp(\dfrac{-27970}{1.987T})P\eta_{eff}}[-2F^0_{CH4}X_{CH4}-(F^0_T+2F^0_{CH4})\ \ln(1-X_{CH4})] = 20\ kg \qquad (33)$$

Because the catalyst particle density is 1750 kg/m³, the catalyst bed volume is calculated to be 23

liters by assuming the voidage is 0.5. The reactor tube used in industrial steam reformers usually

has an inside diameter of 0.07 m and a length of 8 to 10 m. Therefore, the volume of a single

reactor tube is large enough for the demonstration steam reformer.

SECTION 6.0

QUALITY ASSURANCE

The critical parameters involved in this study include catalyst weight, feed rates of gas components, water feed rate, system pressure, reaction temperature, water condensate rate, and offgas flow rate and composition. These parameters, as well as their associated data quality indicator goals for accuracy, are listed in Table 13. This section discusses the quality controls of these measurements.

Catalyst weight was used to calculate the time factor, W/F_{CH4}, which was a parameter affecting methane conversion. The amount of catalyst to be charged into the reactor was weighed by an analytical balance (Mettler AT200). The balance was equipped with built-in calibration weights. According to its manufacturer, the reproducibility is 0.04 mg when the weight of a sample is less than 50 g. This is considered to be sufficiently accurate for catalyst weight measurements.

Carbon and total material balance calculations require accurate measurements of the gas flow rates. The flow rates of individual feed gas components were controlled by Brooks 5850E Mass Flow Controllers (MFC). The accuracy of the MFCs was ± two percent. Because no reliable heat capacity data at high pressures are available for these gas components, each MFC was calibrated by a Gilibrator bubble flow meter using the real working gas under the actual

operating pressure. The accuracy of the Gilibrator bubble flow meter is 0.5 percent. The meter was installed downstream of the SPR back pressure regulator. The pressure and temperature of the bubble meter were recorded and used to correct the readings to the standard conditions (one atm and 25°C). MFC measurements was estimated to be accurate to ±2.5 percent.

The water feed rate was controlled by the HPLC metering pump and measured by a graduated glass tube installed at the inlet of the pump. To measure the feed rate, the water flow was switched from the water reservoir to the graduated tube through a three-way valve. The time needed to remove 10 ml water from the graduated tube was then measured. The estimated accuracy for water flow rate measurement was ± two percent.

The system pressure was controlled by a Grove Mity-Mite Back Pressure Regulator. The pressure in the pressure vessel was measured by a Foxboro/ICT pressure transducer (Model No. 1124-155-A52-A), which was calibrated using a precise pressure gage (Ashcraft, Model No. 45-1082 SX A2-02B-0-1500). The system pressure was maintained within ± 0.2 atm of nominal values.

Three K-type thermocouples, one each at the top, middle, and bottom of the catalyst bed, were used to measure reactor temperature. This temperature was controlled by adjusting the temperature set points of the reactor heating elements. In all the tests, the reaction temperature was controlled ± 5°C of the desired values.

The gas temperature at the exit of the ice-bath was well below 15°C. At that temperature, the water vapor pressure is 0.0168 atm, and the saturated moisture in the offgas at 25 atm should be less than 0.07 mol percent.

The water condensate collected in the trap was discharged and weighed every 30 minutes. A stop watch was used to determine the collection time. The condensate rate thus was equal to the weight of water condensate divided by the collection time. The estimated accuracy of condensate rate measurement was ± 2 percent.

The offgas flow rate was measured by the dry gas meter, which was calibrated by a wet test meter. The accuracy of the dry gas meter was ±1.5 percent.

The GC was calibrated using six standard cylinders. The response factor for each gas component was obtained from a linear regression of the peak areas with known gas compositions. A one-point check was conducted daily before testing to make sure the GC was working properly. Tables 14 and 15 illustrate the data quality of the GC analysis. In each table, the repeated GC results are compared with the known compositions of a standard gas cylinder. The tables include the uncertainties and relative uncertainties calculated from the repeated measurements using Student's t test at a confidence level of 99 percent. The biggest uncertainty in the tables is 1.85 percent for hydrogen measurement, indicating the repeatability of all measurements was quite good. However, it can be seen from the tables that the mean of the measurements for each gas component differs slightly from the actual composition of the standard gas cylinders. These systematical deviations were corrected by the correction factors shown in the tables, which were equal to the known composition divided by the mean of the measurements.

After catalyst activity reached steady state in testing, the data logging usually continued for a few hours to obtain a set of methane conversion data. In most cases, the data were quite

stable. However, the observed data occasionally fluctuated. In these cases, a Chauvenet criterion was used to evaluate the data quality and reject outliers (Holman and Gajda, 1984). Based on the Chauvenet criterion, any data point having a deviation greater than a maximum acceptable value, expressed as a ratio of the deviation to the standard deviation, is considered a false reading and should be eliminated from the data. The Chauvenet criterion is presented in Figure 20 as a function of the total available data points. An example of this type of data checking can be found in Figure 5. Page 4 of Figure 5 showed a standard deviation of 1.88, calculated from all the methane conversion data. The Chauvenet criterion was 1.39, resulting in a maximum acceptable deviation of 2.6. The deviation from the average of each data point was listed in column "**d**". The data points that should be taken out were marked by an "**e**" on their right sides. Page 5 of Figure 5 showed the results after the bad points were eliminated. It can be seen that the standard deviation improved from 1.88 to 0.65 after removing the outliers.

The overall quality of the experimental data in this study was further evaluated by checking carbon and total material balances between the inlet and outlet of the SPR. The calculations were performed using the following equations:

for carbon balance,

$$G_{CH4} + G_{CO} + G_{CO2} = G_{OUT} \ (Y_{CH4} + Y_{CO} + Y_{CO2}) \tag{34}$$

and for total mass balance

$$\sum_i G_i + F_{H2O} = \frac{F_{out}}{22.4} (16.04Y_{CH4} + 28.01Y_{CO} + 44.01Y_{CO2} + 2.016Y_{H2}) + W_{H2O} \qquad (35)$$

where G_i = Mass feed rate of CH_4, CO, CO_2, and H_2, g/min
F_{H2O} = Water feed rate, g/min
F_{out} = Flow rate read from the dry gas meter, l/min
Y_i = Composition from DC analysis
W_{H2O} = Water condensate rate, g/min

The errors in the carbon and total material balances for each experimental run are included in Table 8. It shows that the average error was 1.0 percent for carbon balances and was 1.2 percent for total material balances. The maximum error was 4.7 percent for carbon balances and 6.4 percent for total material balances.

SECTION 7.0

CONCLUSIONS AND RECOMMENDATIONS

This study has successfully demonstrated that the Ni-based catalysts commercially available for conventional steam reforming can be used for the Hynol process to steam reform the biomass gasification product gas with the addition of natural gas feedstock to make synthesis gas for methanol production.

The catalyst has good mechanical strength and allows for the operation at temperatures up to 1000°C.

The hydrogen in the Hynol feed gas assists in preventing carbon formation and maintains the catalyst in the reducing state. An appropriate steam-to-carbon ratio of 2 to 2.5 is recommended for Hynol steam reforming.

Within the range of this study, the carbon monoxide and carbon dioxide in the feed gas have negligible effects on the catalyst activity.

The methane-steam reaction can be well described by a first-order kinetics. The reaction rate is directly proportional to the methane partial pressure. By taking account of the increase in the total flow rate as the reaction proceeds, the intrinsic reaction rate can be expressed by Equation (11).

The intrinsic reaction rate increases with temperature as described by the Arrhenius law. The pre-exponential factor in the rate constant expression is 65552 mol/g-h-atm. The activation energy is 27.97 kcal/mol, which is close to the published data that were measured in the absence of diffusion effects.

The pore diffusion in commercial-size catalyst pellets strongly reduced the catalyst activity. This effect can be quantitatively expressed by the effectiveness factor defined in Equation (30). The effectiveness factor of the Ni-catalyst pellets is a function of reaction temperature and has been correlated by Equation (31). The calculation of the methane conversion over a known weight of catalyst pellets is provided by Equation (32).

A single reactor tube 0.7 m in diameter and 8 m long can be used for the steam pyrolysis reactor in the Hynol demonstration plant.

The experimental equipment used in this study has been demonstrated to be generally suitable for catalyst kinetic studies at high pressures and temperatures. However, the use of more durable heavy-duty heating elements for the test reactor is recommended to avoid unnecessary shutdowns.

Noble metal catalysts, such as rhodium, ruthenium, platinum, and palladium, are tolerable to sulfur poison and are also much more reactive than Ni-based catalysts (Rostrup-Nielsen, 1975). The use of noble metal catalysts for steam reforming in the Hynol process can ease the requirement to clean up the gasification product gas before steam reforming. Sulfur removal from the process gas then can be done before it enters the methanol synthesis reactor where the gas has been cooled. A two-stage technology particularly suitable for removing large amounts of

hydrogen sulfide can be used (Carnell, 1989). The two-stage technology consists of a washing stage followed by a reaction with zinc oxide. Using more active noble metal catalysts allows the use of smaller reactors and, consequently, reduces the capital cost. Therefore, the evaluation of the activity of noble metal catalysts under the Hynol conditions is suggested.

SECTION 8.0

REFERENCES

Acurex Environmental Corporation (1995): Hydrocarb/Hynol Process Demonstration, Final Report A021-1-95, Mountain View, CA.

Agnelli, M.E., Ponzi, E.N., and Yeramian, A.A. (1987): Catalytic Deactivation on Methane Steam Reforming Catalysts. 2. Kinetic Study, Ind. Eng. Chem. Res. **26**, (8), 1707.

Akers, W.W. and Camp, D.P. (1955): Kinetics of the Methane-Steam Reaction, *AIChE Journal*, **1**, (4), 471.

Allen, D.W., Gerhard, E.R., and Likins, M.R. (1975): Kinetics of the Methane-Steam Reaction, *Ind. Eng. Chem. Process Des. Dev.*, **14**, (3), 256.

Bird, R.B., Stewart, W.E., and Lightfoot, E.N. (1960): Transport Phenomena, John Wiley & Sons, New York.

Borgwardt, R.H. (1994): Laboratory Simulation Tests of Hynol Flowsheet D, Memorandum of December 12.

Borgwardt, R.H. (1995): The Hynol Process, Presented at Symposium on Greenhouse Gas Emissions and Mitigation Research, Washington, D.C., June 27-29.

Carnell, P.J.H. (1989): Chapter 4. Feedstock Purification, in **Catalyst Handbook** ed. by Martyn V. Twigg, Second Edition, Wolfe Publishing Ltd, London, England.

Dong, Y. (1994): Kinetic Studies of Steam Reforming, Literature Survey, Acurex Environmental Corporation Project Report, March.

Dong, Y. and Borgwardt, R.H. (1996): Biomass Reactivity in Gasification by the Hynol Process, Preprints of Papers Presented at the 212th ACS National Meeting, Vol. 41, No. 4, Division of Fuel Chemistry, American Chemical Society, Orlando, FL, August 25-29.

Froment, G.F. and Bischoff, K.B. (1979): <u>Chemical Reactor Analysis and Design</u>, John Wiley & Son, New York, p.146.

Gerhard, E.R. and Moe, J.M. (1965): <u>Chemical Reaction and Heat Transfer Rates in the Steam Methane Reaction</u>, AIChE Symposium, Fifty-sixth National Meeting, San Francisco, CA.

Holman, J.P. and Gajda, W.J. (1984): <u>Experimental Methods for Engineers</u>, 4th edition, McGraw-Hill, Inc., New York, p.73.

Liu, J., Wang, F., and Wu, G. (1986): <u>Kinetic Model of CH_4-CO_2-Steam Reaction at High Temperature</u>, *Ind. Eng. Chem. Process Des. Dev.*, **25**, (1), 273.

Motor Vehicle Emission Laboratory (1989): <u>An Analysis of the Economic and Environmental Effects of Methanol as an Automotive Fuel</u>, EPA Report No. 0730 (NTIS PB90-225806), Ann Arbor, MI, September.

Munster, P. And Grabke, H.J. (1981): <u>Kinetics of the Steam Reforming of Methane with Iron, Nickel, and Iron-Nickel Alloys as Catalysts</u>, *Journal of Catalysis*, **72**, 279.

Ridler, D.E. and Twigg, M.V. (1989): <u>Chapter 5. Steam Reforming</u>, in **Catalyst Handbook** ed. by Martyn V. Twigg, Second Edition, Wolfe Publishing Ltd, London, England.

Rostrup-Nielsen, J.R. (1973): <u>Activity of Nickel Catalysts for Steam Reforming of Hydrocarbons</u>, *Journal of Catalysis*, **31**, 173.

Rostrup-Nielsen, J.R. (1975): <u>Steam Reforming Catalysis</u>, Danish Technical Press, Inc., Copenhagen, Denmark, p101.

Steinberg, M. and Dong, Y. (1994): <u>Process and Apparatus for the Production of Methanol from Condensed Carbonaceous Materials</u>, U.S. Patent No. 5,344,848.

Xu, J. and Froment, G.F. (1989): <u>Methane Steam Reforming, Methanation and Water-Gas Shift: I. Intrinsic Kinetics</u>, *AIChE Journal*, **35**, (1), 88.

TABLE 1. ACTIVATION ENERGIES REPORTED IN PREVIOUS WORK

Authors	Catalyst size	P	T	E_A
	mm	atm	°C	cal/mol
Akers & Camp (1955)	3.18	1	640	8,778
Ridler & Twigg (1989)	Foil	1	800-900	31,000
Rostrup-Nielsen (1973)	0.3-0.5	1-31	500	26,200
Munster & Grabke (1981)	N/A	1	700-850	38,000
Liu et al. (1986)	2	1.1	950-1100	12,000
Agnelli et al. (1987)	0.3-0.42	1	640-740	41,600
Xu & Froment (1989)	0.17-0.25	3-15	500-575	57,000

TABLE 2. PURITIES OF THE GASES USED

Gas component	Cylinder grade	Purity %	Cylinder pressure, psi	Cylinder content, m^3
CH_4	Chemically pure	99.0	2,400	10.14
H_2	Ultra-high purity	99.995	2,640	8.24
CO	Chemically pure	99.3	2,000	6.85
CO_2 in H_2	Custom blending	30	2,000	5.63
N_2	Industial	99.998	2,640	8.64

49

TABLE 3. GC AND INTEGRATOR OPERATING CONDITIONS

Item	Setpoint
Initial oven temperature	35°C
Final oven temperature	70°C
Temperature ramp	7.0°C/min
Injector temperature	150°C
TCD temperature	250°C
Carrier gas (He) flow	~30 mL/min
Reference gas flow	~45 mL/min
TCD sensitivity	High
Attenuation	2
Chart speed	1.0 cm/min
Area reject	2000
Threshold	3
Peak width	0.04

TABLE 4. CATALYST PARTICLE DENSITY

CATALYST	Volume	Weight	Density
SAMPLE No.	cm^3	g	g/cm^3
1	1.943	3.4182	1.76
2	1.970	3.4112	1.73
3	1.929	3.3804	1.75
AVERAGE	1.947	3.4033	1.75

50

TABLE 5. CATALYST SOLID DENSITY

Ingredients	ρ_S, g/cm^3	wt.%
Al$_2$O$_3$	4.00	60
MgO	3.65	25
Ni	8.90	15

Catalyst $\rho_S = (4 \times 0.6) + (3.65 \times 0.25) + (8.9 \times 0.15) = 4.65$ g/cm^3

TABLE 6. CATALYST-SPECIFIC SURFACE AREAS AND PORE SIZES

Catalyst	Before Reaction	After Reaction
BET Surface Area (m^2/g)	15.61	16.88
Average Pore Size (Å)	242.16	363.71

TABLE 7. COMPARISON OF CATALYST PROPERTIES

Reference	ρ_S	ρ_P	S	ϕ_S	ϵ
	g/cm^3	g/cm^3	m^2/g	-	-
Agnelli et al. (1987)	2.80	1.02	36	-	0.49
Liu et al. (1986)	2.73	1.89	-	-	0.31
This work	4.65	1.75	15.6	0.39	0.62

Table 8. Experimental data summary.

RUN	Catalyst	W	P	T	FEED GAS FLOW RATE (SLPM)					PRODUCT GAS FLOW RATE (SLPM)					W/F	H_2O/C	$X_{CH4, exp}$	k_{ob}	BALANCES (%)				η_{eff}	$X_{CH4, cal}$
		g	atm	C	H_2	CO	CH_4	CO_2	H_2O	H_2	CO	CH_4	CO_2	H_2O	gh/mol	mol/atm	%	mol/g-h-atm	C	H	O	Total	-	%
R027-6	Powder	1.000	25.1	925	3.181	0.798	3.000	0.360	8.36	6.88	1.08	2.23	0.83	7.25	0.124	2.01	25.67	0.522	-0.43	5.98	1.13	1.49	-	-
R027-7	Powder	1.000	25.0	975	3.181	0.798	3.000	0.360	8.37	7.85	1.37	1.88	0.85	6.93	0.124	2.01	37.33	0.847	-1.39	5.64	1.13	1.24	-	-
R027-8	Powder	1.000	25.0	901	3.181	0.798	3.000	0.360	8.35	6.39	0.98	2.39	0.77	7.41	0.124	2.01	20.33	0.398	-0.43	5.98	0.63	1.17	-	-
R028-4	Powder	1.000	25.0	950	3.181	0.798	3.000	0.360	8.39	7.12	1.22	2.10	0.77	7.20	0.124	2.02	30.00	0.638	-1.64	5.40	0.52	0.77	-	-
R028-5	Powder	1.000	25.0	1000	3.181	0.798	3.000	0.360	8.41	8.37	1.54	1.72	0.85	6.95	0.124	2.02	42.67	1.022	-1.15	6.65	2.64	2.41	-	-
R028-6	Powder	1.000	25.0	901	3.181	0.798	3.000	0.360	8.42	6.40	1.03	2.38	0.75	7.69	0.124	2.03	20.67	0.407	0.05	7.10	2.84	2.87	-	-
R028-7	Powder	1.000	25.0	950	3.181	0.798	3.000	0.358	8.42	7.58	1.29	2.05	0.83	7.20	0.124	2.03	31.67	0.684	0.34	7.25	2.17	2.51	-	-
R028-8	Powder	1.000	24.9	926	3.183	0.798	3.000	0.358	8.44	6.84	1.14	2.24	0.78	7.44	0.124	2.03	25.33	0.521	0.10	6.45	1.87	2.15	-	-
R028-9	Powder	1.000	24.9	1000	3.183	0.798	3.000	0.358	8.41	8.48	1.53	1.73	0.84	6.80	0.124	2.02	42.33	1.015	-1.35	6.52	0.87	1.20	-	-
R032-2-1	Pellet	3.431	25.1	1001	3.181	0.798	3.000	0.360	10.40	5.94	0.89	2.51	0.78	9.56	0.427	2.50	16.33	0.101	0.53	4.80	0.77	1.28	0.097	16.11
R032-2-2	Pellet	3.431	25.1	1001	3.181	0.798	3.000	0.360	8.45	5.95	0.95	2.50	0.73	7.59	0.427	2.03	16.67	0.092	0.53	5.16	0.32	1.05	0.089	17.80
R032-3	Pellet	3.431	25.0	1001	4.699	0.633	3.523	0.431	9.98	6.56	0.85	3.00	0.72	9.25	0.364	2.18	14.85	0.099	-0.37	0.38	0.54	0.33	0.095	14.88
R032-4	Pellet	3.431	25.0	1001	5.476	0.736	4.113	0.503	11.62	7.34	0.96	3.58	0.80	10.88	0.311	2.17	12.96	0.100	-0.22	0.23	0.58	0.36	0.096	12.96
R032-6	Pellet	3.431	25.0	1002	3.181	0.798	3.000	0.360	8.38	5.88	0.89	2.47	0.65	7.84	0.427	2.02	17.67	0.099	-3.56	6.26	1.33	1.03	0.094	17.87
R034-2	Pellet	3.339	25.0	951	3.931	0.529	2.935	0.350	10.41	5.43	0.61	2.55	0.67	9.80	0.425	2.73	13.12	0.084	0.42	0.61	1.00	0.83	0.126	13.13
R034-3	Pellet	3.339	25.2	901	3.931	0.529	2.935	0.350	10.48	5.41	0.57	2.61	0.70	9.98	0.425	2.75	11.07	0.069	1.73	1.61	2.03	1.91	0.170	11.40
R034-4	Pellet	3.339	25.2	1000	4.175	0.529	2.935	0.000	10.78	6.23	0.58	2.49	0.45	10.07	0.425	3.11	15.16	0.099	1.62	2.17	2.09	2.02	0.096	15.22
R034-5	Pellet	3.339	25.0	1001	4.175	0.529	2.935	0.000	8.57	6.18	0.65	2.45	0.42	7.72	0.425	2.47	16.52	0.097	1.62	0.99	1.22	1.24	0.093	16.95
R034-6	Pellet	3.339	25.0	1000	3.931	0.529	2.935	0.350	10.49	5.65	0.68	2.50	0.67	9.73	0.425	2.75	14.82	0.096	0.94	0.44	0.26	0.39	0.093	15.24
R035-1	Pellet	3.228	25.0	1001	3.810	0.529	2.935	0.350	10.50	5.67	0.66	2.50	0.68	9.97	0.411	2.75	14.82	0.099	0.68	2.28	2.23	1.97	0.095	14.92
R036-3	Pellet	3.234	25.0	902	4.175	0.529	2.935	0.000	8.26	5.20	0.52	2.60	0.27	7.86	0.411	2.38	11.41	0.065	-2.14	-0.25	1.49	0.50	0.159	12.46
R036-4	Pellet	3.234	25.1	901	3.931	0.529	2.935	0.350	10.37	4.77	0.54	2.58	0.55	9.92	0.411	2.72	12.10	0.079	-3.78	-1.59	-0.34	-1.11	0.193	11.08
R036-5	Pellet	3.234	25.1	901	3.678	0.529	2.935	0.697	10.41	4.50	0.57	2.58	0.86	9.99	0.411	2.50	12.10	0.079	-3.63	-1.54	-0.43	-1.15	0.195	11.01
R036-6	Pellet	3.234	25.0	902	3.931	0.000	2.935	0.350	10.43	4.77	0.18	2.58	0.42	10.08	0.411	3.18	12.10	0.077	-3.20	-1.09	-0.27	-0.85	0.187	11.35
R036-8	Pellet	3.234	25.1	899	3.943	0.529	2.935	0.338	10.30	4.99	0.51	2.60	0.56	9.74	0.411	2.71	11.41	0.074	-3.47	-0.91	-1.17	-1.53	0.185	11.05
R036-10	Pellet	3.234	25.0	903	3.589	0.529	2.935	0.000	10.34	4.89	0.49	2.59	0.30	9.57	0.411	2.98	11.75	0.074	-2.42	-0.80	-1.92	-1.84	0.177	11.53
R037-1	Pellet	3.195	25.1	953	3.181	0.798	3.000	0.359	8.67	4.84	0.77	2.61	0.82	7.76	0.398	2.09	13.00	0.076	1.03	-0.17	-0.16	0.07	0.113	14.22
R037-2	Pellet	3.195	25.1	953	3.181	0.798	3.000	0.359	12.46	4.66	0.71	2.69	0.80	11.19	0.398	3.00	10.33	0.073	1.03	-1.90	-3.41	-2.51	0.108	11.77
R038-2	Pellet	3.162	25.0	1001	3.181	0.799	3.000	0.359	10.37	5.41	0.79	2.54	0.81	9.41	0.393	2.49	15.33	0.103	-0.43	1.81	-0.52	-0.19	0.098	14.94
R038-4	Pellet	3.162	25.0	1000	3.181	1.598	3.000	0.359	10.45	5.36	1.30	2.55	1.10	9.09	0.393	2.11	15.00	0.105	-0.14	-0.40	-1.36	-1.01	0.102	14.26
R038-5	Pellet	3.162	25.0	1000	3.181	0.400	3.000	0.359	10.51	5.35	0.59	2.50	0.75	9.25	0.393	2.80	16.67	0.111	2.15	-0.46	-2.48	-1.42	0.107	15.08
R038-6	Pellet	3.162	25.0	1000	3.181	0.000	3.000	0.359	10.39	5.12	0.35	2.53	0.52	9.52	0.393	3.09	15.67	0.101	1.22	0.66	-1.78	-0.95	0.097	15.48

(Continued)

52

Table 8. Experimental data summary. (continued)

RUN	Catalyst	W	P	T	FEED GAS FLOW RATE (SLPM)					PRODUCT GAS FLOW RATE (SLPM)					W/F	H_2O/C	X_{CH4}	k_{ob}	BALANCES (%)				η_{eff}	$X_{CH4, cat}$
		g	atm	C	H_2	CO	CH_4	CO_2	H_2O	H_2	CO	CH_4	CO_2	H_2O	gh/mol	mol/atm	%	mol/g-h-atm	C	H	O	Total	-	%
R039-2	Pellet	3.204	25.1	950	4.000	0.799	3.000	0.359	10.42	5.76	0.78	2.63	0.76	9.42	0.399	2.51	12.33	0.083	0.29	0.10	-1.82	-1.18	0.126	12.39
R039-3	Pellet	3.204	25.1	950	1.999	0.799	3.000	0.359	10.42	3.84	0.67	2.60	0.87	9.28	0.399	2.51	13.33	0.081	-0.43	-0.53	-2.06	-1.57	0.123	13.71
R039-4	Pellet	3.204	25.0	949	3.181	0.799	3.000	0.359	10.46	4.49	0.73	2.64	0.79	9.42	0.399	2.52	12.00	0.078	0.05	-2.30	-2.06	-1.73	0.119	12.79
R039-5	Pellet	3.204	25.1	951	1.098	0.799	3.000	0.359	10.40	2.81	0.63	2.71	0.90	9.30	0.399	2.50	9.67	0.054	1.97	0.20	-1.54	-0.69	-	-
R041-2	Pellet	3.275	25.2	903	3.181	0.799	3.000	0.359	9.69	4.79	0.85	2.64	0.63	8.90	0.408	2.33	12.00	0.072	-0.91	0.52	-1.76	-1.28	0.174	11.97
R041-3	Pellet	3.275	25.0	903	1.098	0.799	3.000	0.359	9.75	2.56	0.81	2.73	0.66	9.04	0.408	2.34	9.00	0.047	1.01	1.26	-0.86	-0.24	-	-
R041-4	Pellet	3.275	25.0	905	3.181	0.799	3.000	0.359	9.41	4.55	0.84	2.64	0.54	8.70	0.408	2.26	12.00	0.072	-3.32	-0.33	-2.81	-2.56	0.169	12.14
R041-5	Pellet	3.275	25.0	903	1.999	0.799	3.000	0.359	9.17	3.34	0.81	2.69	0.61	8.67	0.408	2.21	10.33	0.056	-1.15	1.29	0.12	0.02	-	-
R041-6	Pellet	3.275	24.9	901	1.098	0.799	3.000	0.359	9.22	2.54	0.79	2.72	0.62	8.63	0.408	2.22	9.33	0.048	-0.67	1.79	-0.72	-0.39	-	-
R041-7	Pellet	3.275	25.1	901	4.000	0.799	3.000	0.359	9.18	5.40	0.84	2.63	0.53	8.62	0.408	2.21	12.33	0.076	-3.80	0.52	-1.65	-1.75	0.187	11.66
R041-8	Pellet	3.275	25.1	901	0.838	0.799	3.000	0.359	9.19	2.60	0.78	2.65	0.63	8.68	0.408	2.21	11.67	0.059	-2.36	3.44	0.12	0.05	-	-
R042-2	Pellet	3.115	25.1	900	3.184	0.799	3.000	0.355	9.19	5.00	0.84	2.64	0.58	8.15	0.388	2.21	12.00	0.074	-2.26	0.30	-5.13	-3.81	0.184	11.59
R042-3	Pellet	3.115	25.0	900	0.841	0.799	3.000	0.355	9.20	2.55	0.81	2.66	0.65	8.02	0.388	2.21	11.33	0.060	-0.82	-0.94	-5.41	-3.95	-	-
R042-4	Pellet	3.115	25.0	901	1.061	0.799	3.000	0.355	9.17	2.43	0.82	2.67	0.61	8.25	0.388	2.21	11.00	0.059	-1.30	-1.30	-3.64	-2.89	-	-
R042-5	Pellet	3.115	25.0	901	4.004	0.799	3.000	0.355	9.09	5.67	0.87	2.76	0.52	7.69	0.388	2.19	8.00	0.050	-0.10	-1.12	-9.43	-6.39	-	-
R044-1	Pellet	3.123	25.1	900	3.184	0.799	3.000	0.355	8.38	4.45	0.72	2.70	0.71	7.90	0.389	2.02	10.00	0.058	-0.58	1.06	1.53	1.02	0.143	12.16
R044-2	Pellet	3.123	25.1	950	3.184	0.799	3.000	0.355	8.34	4.72	0.76	2.65	0.70	7.76	0.389	2.01	11.67	0.068	-1.06	1.46	0.72	0.45	0.103	14.07
R044-3	Pellet	3.123	25.1	1000	3.184	0.799	3.000	0.355	8.35	4.76	0.76	2.56	0.71	7.74	0.389	2.01	14.67	0.087	-2.99	0.49	0.62	-0.15	0.085	16.41
R045-6	Pellet	3.150	25.0	950	3.184	0.799	1.000	0.355	9.29	3.98	0.57	0.84	0.71	8.42	1.176	4.31	16.00	0.088	-1.58	-2.72	-3.60	-3.27	-	-
R045-7	Pellet	3.150	25.0	951	3.184	0.799	3.000	0.355	9.29	4.63	0.72	2.57	0.74	8.29	0.392	2.24	14.33	0.090	-2.99	-2.24	-2.86	-2.81	0.135	13.46
R046-4	Pellet	3.203	24.9	951	3.179	0.799	1.000	0.360	9.23	4.64	0.58	0.84	0.76	8.52	1.196	4.28	16.00	0.086	0.97	2.99	-1.20	-0.43	-	-
R046-7	Pellet	3.203	25.0	950	3.179	0.799	2.000	0.360	9.24	5.02	0.65	1.72	0.77	8.36	0.598	2.92	14.00	0.080	-0.60	2.44	-1.94	-1.15	-	-
R046-9	Pellet	3.203	24.9	951	3.179	0.799	3.000	0.360	9.25	5.36	0.75	2.58	0.78	8.21	0.399	2.22	14.00	0.086	-1.18	1.63	-2.31	-1.54	0.130	13.64
																	Average		-0.84	0.19	-1.39	-1.09		

TABLE 9. BLANK TEST RESULTS (PR-09)

Time	CH_4 IN	Out Rate	CH_4	CH_4 OUT	Δ CH4
	SLPM	L/min	%	L/min	%
1:00	3.14	11.80	28.68	3.38	7.64
1:30	3.14	11.06	27.98	3.09	-1.59
2:00	3.14	11.06	28.36	3.14	0.00
2:30	3.14	11.36	26.42	3.00	-4.46
3:00	3.14	10.93	28.00	3.06	-2.55
3:30	3.14	11.53	26.88	3.10	-1.27
4:00	3.14	10.95	27.74	3.04	-3.18
Average	3.14	11.24	27.72	3.12	-0.64

TABLE 10. TEMPERATURE DEPENDENCE OF CATALYST POWDERS.
(25 ATM, HYNOL FEED GAS, W/F = 0.124 G-H/MOL, H2O/C = 2)

RUN No.	T	X_{CH4}	k_1
	°C	%	mol/g-h-atm
R027-8	901	20.33	0.398
R028-6	901	20.67	0.407
R027-6	925	24.67	0.522
R028-8	926	25.33	0.521
R028-4	950	30.00	0.638
R028-7	950	31.00	0.684
R027-7	975	36.67	0.847
R028-5	1001	42.67	1.022
R028-9	1000	42.33	1.015

54

TABLE 11. TRANSPORT PROPERTIES OF GAS COMPONENTS

Property	CH_4	H_2	CO	CO_2	H_2O	Mixture
Rate, SLPM	3.00	3.181	0.799	0.359	8.330	15.669
P_i, **atm**	4.79	5.08	1.27	0.57	13.29	25.0
Pc, atm	46	13.1	35	73.8	220.5	-
Tc, atm	190.6	33.2	132.9	304.2	647.3	-
M_i, **g/mol**	16.04	2.016	28.01	44.01	18.016	15.50
$\rho_i \times 10^3$, **g/cm³**	3.84	0.48	6.70	10.53	4.31	3.71
$\mu_i \times 10^3$, **g/cm-s**	3.219	1.996	4.777	4.966	3.405	3.497
D_{CH4-i}, **cm²/s**	-	0.417	0.122	0.097	0.289	0.263

TABLE 12. EFFECTIVENESS FACTORS OF CATALYST PELLETS

T, °C	900	950	1000
Average	0.177	0.127	0.096
Minimum	0.167	0.119	0.092
Maximum	0.186	0.134	0.099
sd	0.010	0.008	0.003

TABLE 13. DATA QUALITY INDICATOR GOALS FOR ACCURACY

Parameter	Quality Objective	QC Methods
Catalyst weight	Accuracy: ± 0.01 percent	Mettler AT200 analytical balance used
Feed rates of CH4, H2, CO and CO2	Accuracy: ± 2 percent	MFCs are calibrated at high operating pressures
Water feed rate	Accuracy: ± 2 percent	HPLC pump used and calibrated during runs
System pressure	Accuracy: ± 0.2 kg/cm^2	Mity-Mite S-91 W back pressure regulator used
Reaction temperature	Accuracy: ± 5 °C	LabTech Control software used for temperature controlling
Condensates rate	Accuracy: ± 2 percent (estimate)	Calculated from the condensate weight collected and the time recorded by stopwatch for water accumulation
Offgas flow rate	Accuracy: ± 1.5 percent	Dry gas meter is calibrated
Offgas composition	Accuracy: ± 2 percent	A QA check is run on the GC daily

56

TABLE 14. DATA QUALITY OF GC ANALYSIS (GAS CYLINDER No. 5)

Calibration Date: 5/20/96					
Gas #5	H2	N2	CO	CH4	CO2
%	76.30	2.01	4.90	12.80	3.99
Cor. Factor	0.992	0.987	0.992	0.998	0.988
GC Run					
1	73.17	2.01	4.96	12.87	4.15
2	72.46	2.05	4.99	12.91	4.05
3	78.37	2.14	5.01	12.99	4.03
4	78.55	2.07	4.99	12.99	4.04
5	76.22	2.01	4.94	12.85	4.04
6	78.21	2.06	4.95	12.87	4.01
7	77.47	2.00	4.92	12.77	4.02
8	75.71	2.03	4.93	12.84	4.01
9	77.44	2.01	4.93	12.81	4.06
10	76.69	2.04	4.91	12.76	4.03
11	78.52	2.03	4.91	12.77	4.02
12	75.43	2.03	4.93	12.74	4.01
13	74.42	2.05	4.92	12.78	4.02
14	80.17	2.05	4.98	12.87	4.07
15	78.77	2.01	4.90	12.75	4.00
16	75.75	2.02	4.92	12.75	4.03
17	75.08	2.03	4.93	12.84	4.03
18	79.85	2.02	4.93	12.79	4.04
19	78.71	2.01	4.90	12.76	4.02
20	77.20	2.08	4.94	12.78	4.09
Average	76.91	2.04	4.94	12.82	4.04
sd	2.20	0.04	0.05	0.08	0.06
Uncertainty	1.41	0.03	0.03	0.05	0.04
U, %	1.85	1.36	0.65	0.39	0.96

TABLE 15. DATA QUALITY OF GC ANALYSIS (GAS CYLINDER No. 6)

Calibration Date: 7/23/96					
Gas #6	H2	N2	CO	CH4	CO2
%	52.61	10.50	24.70	5.10	7.09
Cor. Factor	1.006	0.994	0.994	1.017	1.013
GC Run					
1	52.36	10.52	24.73	4.97	7.04
2	52.75	10.47	24.70	4.99	6.98
3	52.85	10.53	24.76	5.00	7.13
4	52.10	10.46	24.60	4.98	6.89
5	52.67	10.52	24.74	4.99	7.01
6	52.61	10.47	24.70	5.00	7.02
7	53.76	10.49	24.75	5.02	6.93
8	50.88	10.59	24.89	5.01	6.96
9	51.26	10.67	25.08	5.08	7.09
10	51.55	10.63	25.06	5.06	7.11
11	52.39	10.59	24.99	5.05	6.98
12	52.28	10.71	25.06	5.08	7.01
13	52.00	10.78	24.92	5.03	6.95
14	52.68	10.54	24.89	5.01	7.03
15	52.87	10.56	24.82	5.00	7.00
16	53.28	10.58	24.89	5.02	7.02
17	52.56	10.58	24.86	5.00	7.03
18	51.24	10.55	24.76	4.99	6.82
19	52.00	10.51	24.78	4.99	6.93
20	52.20	10.54	24.76	4.99	6.99
Average	52.31	10.56	24.84	5.01	7.00
sd	0.77	0.10	0.19	0.10	0.12
Uncertainty	0.49	0.07	0.12	0.06	0.08
U, %	0.93	0.64	0.50	1.19	1.09
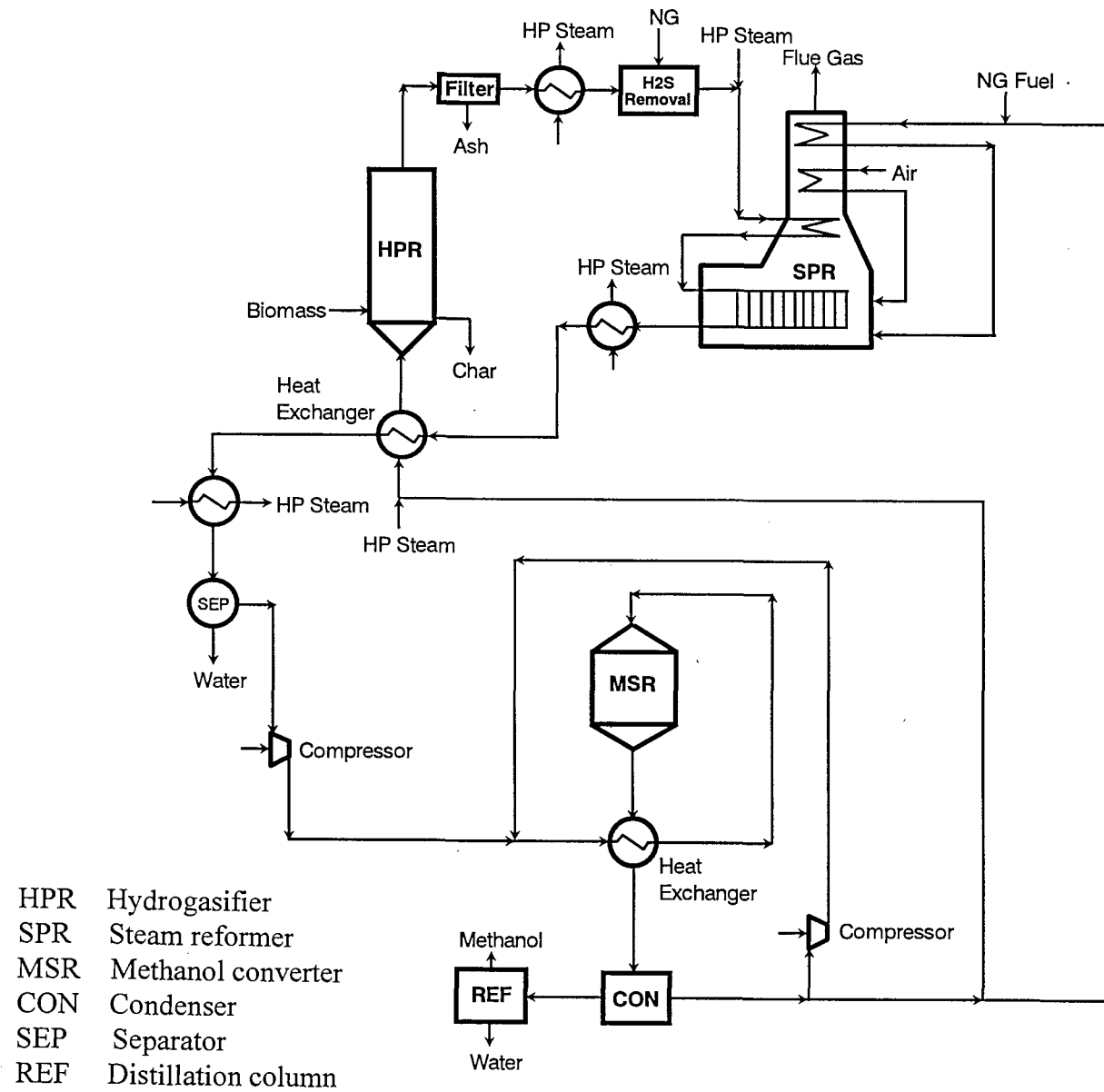
Figure 1. Hynol process flowsheet.

HPR   Hydrogasifier
SPR   Steam reformer
MSR   Methanol converter
CON   Condenser
SEP   Separator
REF   Distillation column
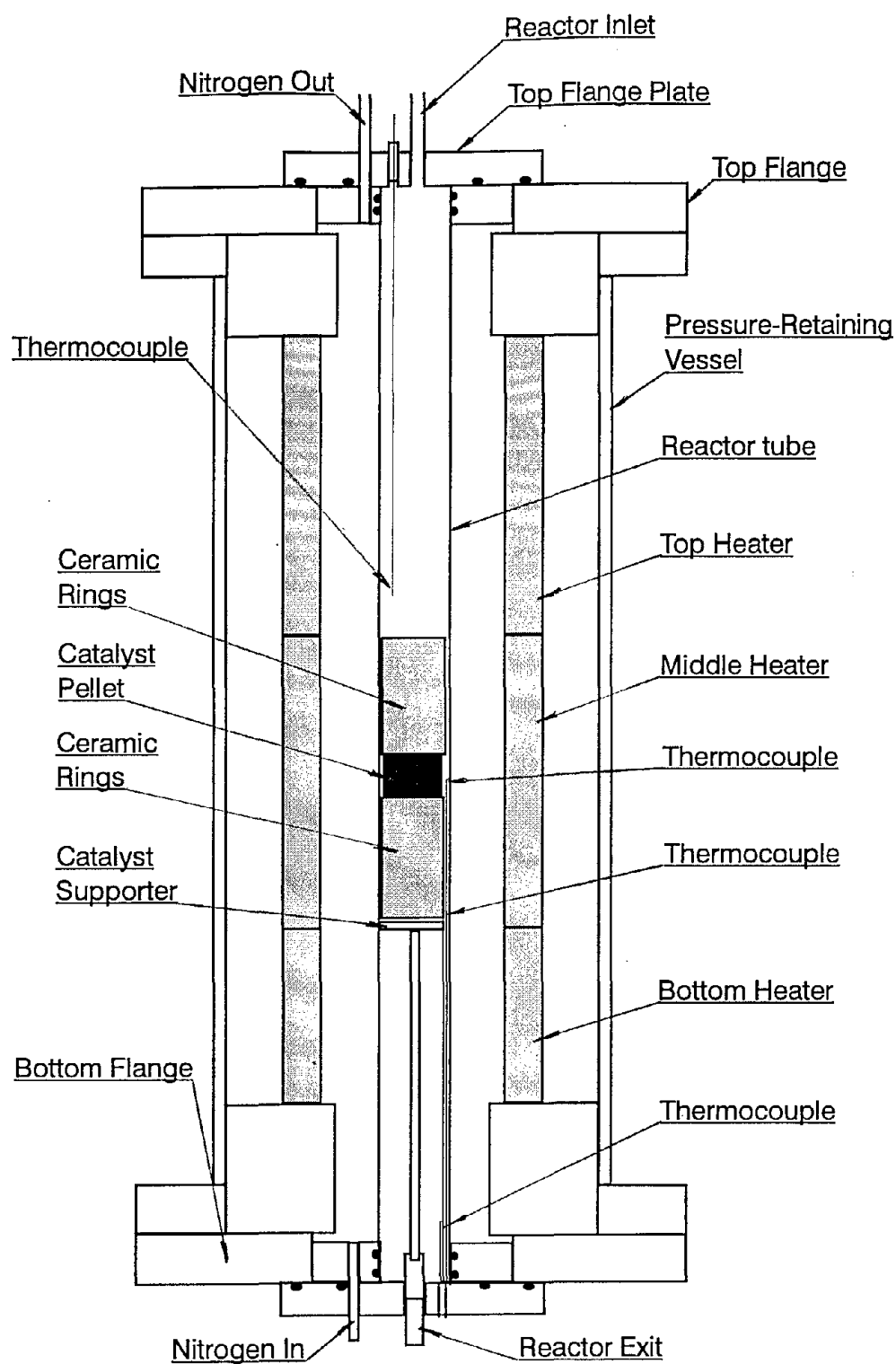
Figure 2. Schematic diagram of the steam reforming reactor.
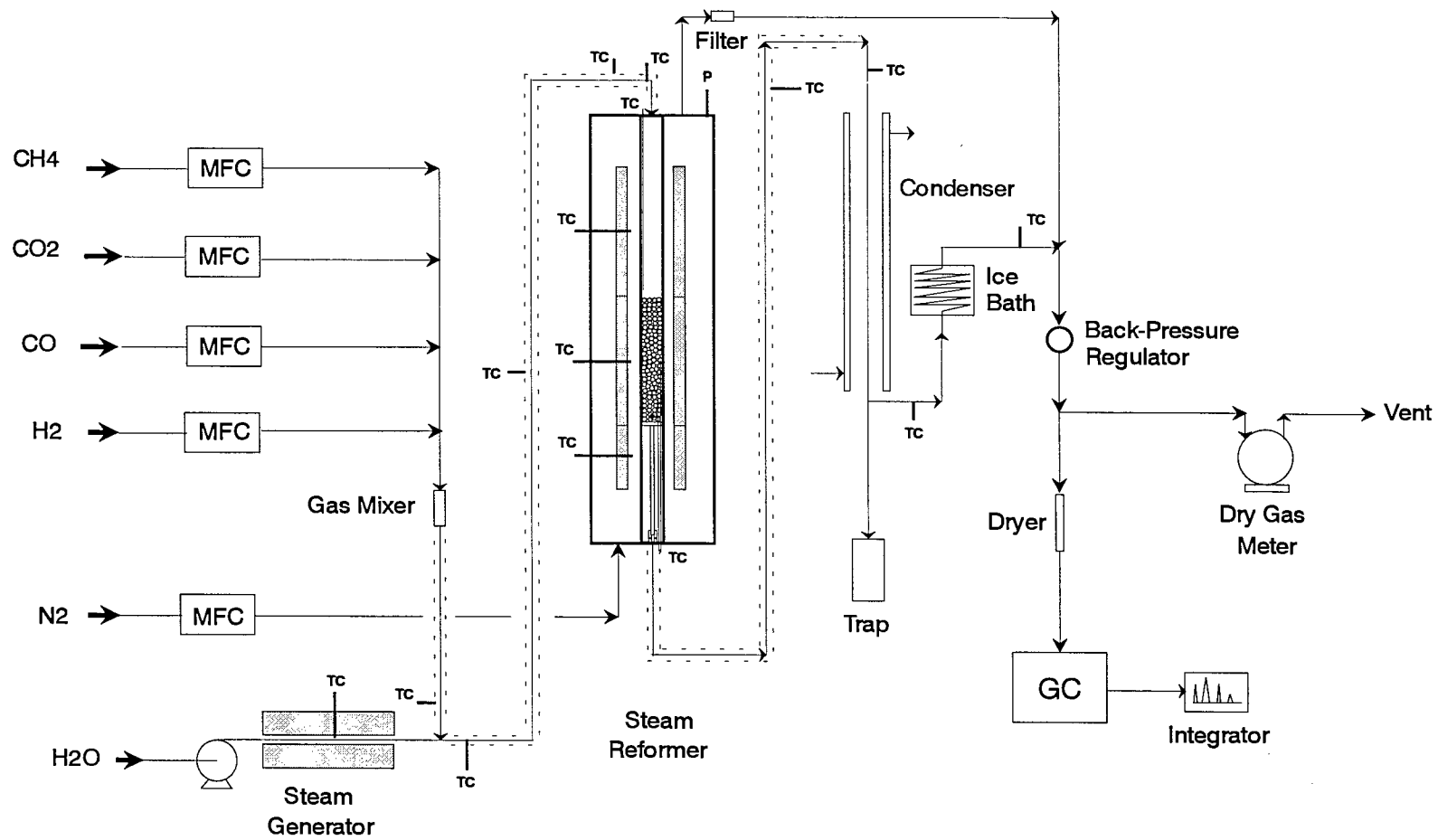
Figure 3. Flowsheet of the experimental equipment.
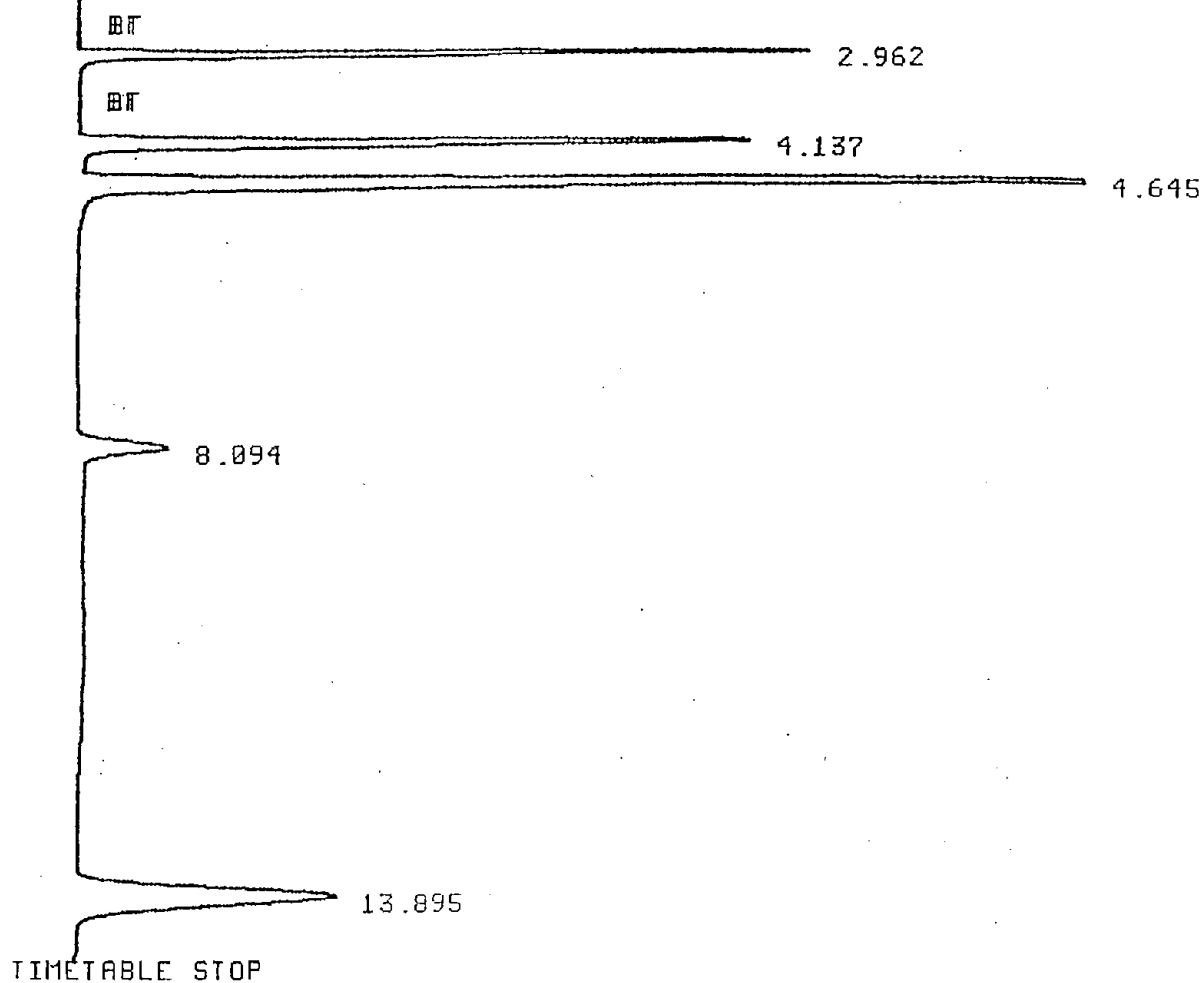
```
START;

              ⊞T
                                                              2.962
              ⊞T
                                                       4.137
                                                                    4.645




                        8.094




                        13.895
        TIMETABLE STOP


Closing signal file A:Q225494E.BNC
Storing report to A:Q225494E.RPT

RUN#     97          FEB 14, 1996  15:27:09

ESTD-AREA
      RT TYPE        AREA  WIDTH CAL# MOLAR%       NAME
   2.962 N PB        41898  .067   1R    66.632    H2
   4.137   PB       473356  .103   2R     8.962    N2
   4.645   BB       942094  .120   3R    17.329    CO
   8.094   PB       104680  .179   4R     2.132    CH4
  13.895   BB       490682  .278   5R     6.244    CO2

TOTAL AREA=2052710
MUL FACTOR=1.0000E+00
```

Figure 4. Typical printout of the the GC integrator.

SPR DATA SHEET

RUN No:	R028-4																Page 1
DATE:	7/12																
GC CHECK:		H$_2$	N$_2$	CO	CH$_4$	CO$_2$		Calibration Date		5/20/96							
	Gas #5	76.300	2.010	4.900	12.800	3.990											
	GC	79.849	2.015	4.925	12.792	4.042											
	Error%	4.65	0.25	0.51	-0.06	1.30											
Correction Factor:		0.994	0.988	0.992	0.998	0.989											
GC	Run																
	1	73.167	2.012	4.956	12.871	4.146											
	2	72.462	2.047	4.988	12.908	4.048											
	3	78.365	2.135	5.009	12.988	4.030											
	4	78.554	2.074	4.987	12.986	4.043											
	5	76.216	2.007	4.941	12.853	4.042											
	6	78.212	2.056	4.947	12.868	4.008											
	7	77.473	1.996	4.918	12.769	4.018											
	8	75.711	2.030	4.933	12.843	4.006											
	9	77.444	2.006	4.933	12.810	4.063											
	10	76.688	2.036	4.909	12.759	4.033											
	11	78.522	2.034	4.912	12.768	4.024											
	12	75.430	2.025	4.927	12.742	4.009											
	13	74.424	2.054	4.919	12.780	4.021											
	14	80.167	2.045	4.978	12.868	4.067											
	15	78.766	2.005	4.895	12.747	3.997											
	16	75.753	2.016	4.915	12.752	4.029											
	17	75.083	2.033	4.932	12.837	4.025											
	18	79.849	2.015	4.925	12.792	4.042											
	19																
	20																
	Average	76.794	2.035	4.940	12.830	4.036											
	sd	2.182	0.033	0.032	0.076	0.033											

Figure 5. Example of SPR data sheets (page 1).

SPR DATA SHEET

RUN No:	R028-4				Catalyst Type:	HT		Diluent Type:	CR				Page 2
DATE:	7/12				W (g):	1.00		Diluent (g):	90				
					Dp (mm):								

EXPERIMENTAL CONDITIONS

HEATE	Set			Gas Rate (SLPM)					Balance N_2 (SLPM)				
SG	400				Set Poin	Actual			set				
OUTLET	400			CH_4	2.785	3.000			0.10				
IN #1	450			H_2	2.726	2.342							
IN #2	650			CO	0.700	0.798							
IN #3	650			CO_2	1.089	1.199	CO2%	30.0					

DATA:

Time	P	SG	INLET	REACTOR				OUTLET	ICE BATH			HEATER ACTUAL			
H:M	atm	T201	T202	T203	T204	T205	T207	T208	T112	T113	SG	OUTLET	H212	H213	H214
9:00	25.02	294	380	950	950	952	478	369	19	9	377	398	923	900	793
9:30	25.02	333	381	950	950	950	496	365	19	9	434	398	924	903	804
10:00	25.02	357	381	951	950	950	516	371	19	10	452	401	923	904	800
10:30	25.02	327	381	952	951	950	500	370	20	11	402	400	923	906	801
11:00	25.02	342	382	949	950	951	476	369	20	11	445	400	923	909	802
11:30	25.02	346	381	948	952	954	533	370	21	11	411	400	925	910	804
12:00	25.02	328	381	950	952	950	475	368	21	11	412	398	926	910	803
12:30	25.02	355	381	948	950	950	489	370	21	11	459	400	926	908	805
13:00	24.99	319	381	950	951	950	482	367	21	11	391	398	927	909	805
13:30	24.99	344	381	951	951	951	479	366	21	11	439	398	927	909	804
14:00	24.99	350	382	949	950	950	534	371	21	11	430	405	926	906	810
14:30	24.94	332	381	948	950	950	485	367	22	12	413	398	929	909	807
END															

64

Figure 5. Example of SPR data sheets (page 2).

SPR DATA SHEET

RUN No.	R028-4																Page 3
Date		7/12															
Time	FI-101	ΔP	T	Dry Gas		Trap Water				Water In			Product Gas (mol%)				
H:M	sec/.3cf	in H2O	°C	l/min	g	min.	sec.	g/min	set	s/10ml	ml/min	H2	N2	CO	CH4	CO2
9:00	40.5	1.9	23	12.79	190.4	31	42	6.01	6.10	89.2	6.73	60.359	10.006	10.419	15.908	6.371
9:30	41.5	1.8	23	12.45	152.3	27	19	5.58	6.10	89.1	6.73	60.601	8.423	10.494	16.779	6.425
10:00	42.5	1.8	23	12.16	193.3	31	47	6.08	6.10	89.0	6.74	59.437	9.313	9.021	18.101	6.915
10:30	43.0	1.8	23	12.02	148.5	26	39	5.57	6.10	88.9	6.75	59.508	7.074	10.659	17.323	6.506
11:00	43.2	1.8	23	11.96	190.3	32	13	5.91	6.10	89.0	6.74	61.540	6.741	10.504	17.406	6.678
11:30	43.7	1.8	24	11.81	191.7	31	13	6.14	6.10	88.6	6.77	58.835	9.095	9.570	18.146	6.831
12:00	43.7	1.8	24	11.79	156.0	28	56	5.39	6.10	88.5	6.78	61.061	6.543	10.559	17.836	6.575
12:30	44.1	1.8	24	11.68	196.0	32	20	6.06	6.10	88.9	6.75	61.740	6.169	10.402	18.157	6.829
13:00	44.6	1.7	25	11.52	147.7	27	24	5.39	6.10	89.3	6.72	59.108	6.152	10.544	18.117	6.612
13:30	44.3	1.7	25	11.60	190.2	30	58	6.14	6.10	89.1	6.73	60.561	6.192	10.558	18.084	6.578
14:00	44.0	1.7	25	11.68	183.4	29	34	6.20	6.10	88.8	6.76	59.222	8.282	9.181	19.190	6.896
14:30	44.2	1.7	25	11.61	150.7	27	18	5.52	6.10	89.1	6.73	62.046	6.075	10.573	18.080	6.611
END																

65

Figure 5. Example of SPR data sheets (page 3).

SPR DATA SHEET

RUN No.	R028-4			P atm	25.0											Page 4
Date		7/12														

INPUT	H2	CO	CH4	CO2	H2O	Total		C				H2O/C		W/F	
	SLPM	SLPM	SLPM	SLPM	SLPM	SLPM		atom				mol/mol		gh/mol	
Rate	3.181	0.798	3.000	0.360	8.386	15.725		0.186				2.02		0.12	
p, atm	5.06	1.27	4.77	0.57	13.34	25.01									

		In	Output												
t	T_{av}	H2O	CO	CH4	CO2	H2	H2O	X_{CH4}		d		dC	dH	dO	Total
hr	°C	l/min	l/min	l/min	l/min	l/min	l/min	%				%	%	%	%
0.5	951	8.36	1.32	2.03	0.81	7.67	7.47	32.36		2.69	e	-0.05	9.40	5.25	4.77
1.0	950	8.37	1.30	2.08	0.79	7.50	6.93	30.51		0.85		0.33	5.96	-0.81	0.41
1.5	950	8.38	1.09	2.20	0.83	7.18	7.56	26.81		2.86	e	-1.03	8.94	4.17	3.80
2.0	951	8.39	1.27	2.08	0.77	7.11	6.93	30.77		1.10		-0.90	3.50	-1.66	-0.75
2.5	950	8.38	1.25	2.08	0.79	7.31	7.34	30.76		1.09		-1.08	7.11	2.73	2.59
3.0	952	8.42	1.12	2.14	0.80	6.90	7.64	28.76		0.90		-2.48	6.87	4.15	3.19
3.5	951	8.43	1.23	2.10	0.77	7.15	6.70	30.10		0.43		-1.46	2.48	-4.80	-3.06
4.0	950	8.39	1.20	2.12	0.79	7.16	7.54	29.49		0.18		-1.19	7.73	4.13	3.57
4.5	951	8.35	1.21	2.08	0.75	6.77	6.70	30.57		0.90		-2.80	0.58	-4.63	-3.50
5.0	951	8.37	1.22	2.09	0.75	6.98	7.64	30.22		0.56		-2.29	7.13	4.76	3.66
5.5	950	8.40	1.06	2.24	0.80	6.87	7.71	25.45		4.22	e	-1.47	8.40	4.54	3.87
6.0	950	8.37	1.22	2.09	0.76	7.16	6.86	30.20		0.53		-2.11	3.73	-2.95	-1.81
Ave	950	8.39	1.21	2.11	0.78	7.15	7.25	29.67		2.60					
sd								1.88							
Chau								1.39							
Carbon loss (g/h)		0.00													
END															

Figure 5. Example of SPR data sheets (page 4).

SPR DATA SHEET

RUN No.	R028-4			P atm	25.0											Page 5
Date		7/12														
INPUT	H2	CO	CH4	CO2	H2O	Total		C				H2O/C		W/F		
	SLPM	SLPM	SLPM	SLPM	SLPM	SLPM		atom				mol/mol		gh/mol		
Rate	3.181	0.798	3.000	0.360	8.386	15.725		0.186				2.02		0.12		
p, atm	5.06	1.27	4.77	0.57	13.34	25.01										

		In	Output												
t	T_{av}	H2O	CO	CH4	CO2	H2	H2O	X_{CH4}		d		dC	dH	dO	Total
hr	°C	l/min	l/min	l/min	l/min	l/min	l/min	%				%	%	%	%
0.5															
1.0	950	8.37	1.30	2.08	0.79	7.50	6.93	30.51		0.36		0.33	5.96	-0.81	0.41
1.5															
2.0	951	8.39	1.27	2.08	0.77	7.11	6.93	30.77		0.62		-0.90	3.50	-1.66	-0.75
2.5	950	8.38	1.25	2.08	0.79	7.31	7.34	30.76		0.61		-1.08	7.11	2.73	2.59
3.0	952	8.42	1.12	2.14	0.80	6.90	7.64	28.76		1.39		-2.48	6.87	4.15	3.19
3.5	951	8.43	1.23	2.10	0.77	7.15	6.70	30.10		0.05		-1.46	2.48	-4.80	-3.06
4.0	950	8.39	1.20	2.12	0.79	7.16	7.54	29.49		0.67		-1.19	7.73	4.13	3.57
4.5	951	8.35	1.21	2.08	0.75	6.77	6.70	30.57		0.41		-2.80	0.58	-4.63	-3.50
5.0	951	8.37	1.22	2.09	0.75	6.98	7.64	30.22		0.07		-2.29	7.13	4.76	3.66
5.5															
6.0	950	8.37	1.22	2.09	0.76	7.16	6.86	30.20		0.04		-2.11	3.73	-2.95	-1.81
Ave	950	8.39	1.22	2.10	0.77	7.12	7.14	30.15		0.91					
sd								0.65							
Chau								1.39							
Carbon loss (g/h)		0.00													
END															

Figure 5. Example of SPR data sheets (page 5).

CO 2.51
CO2 1.13
CH4 5.68
H2O 4.17
H2 10.00
N2 0.53

CH4 3.75 mol   Steam 6.65 mol

100 kg dry biomass
11.1 kg moisture

Gasifier

24.02 mol

Reformer

Carbon 0.085 mol

CO 1.94
CO2 0.57
CH4 2.42
H2O 2.41
H2 14.10
N2 0.53
MeOH 0.23

22.2 mol

48.4 mol

H2O 3.85 mol

CO 9.83
CO2 0.80
CH4 2.44
H2O 0.31
H2 30.67
N2 0.53

44.6 mol

Steam 2.4 mol

Purge 0.2 mol   167 mol

CO 18.3
CO2 5.4
CH4 22.9
H2O 0.13
H2 133.5
N2 5.0
MeOH 2.17

187 mol

CO 18.3
CO2 5.4
CH4 22.9
H2O 0.7
H2 133.5
N2 5.0
MeOH 10.0

212 mol

MeOH 7.87 mol

Condenser

H2O 0.51 mol

196 mol

Methanol Converter

Figure 6. Hynol process simulation results.
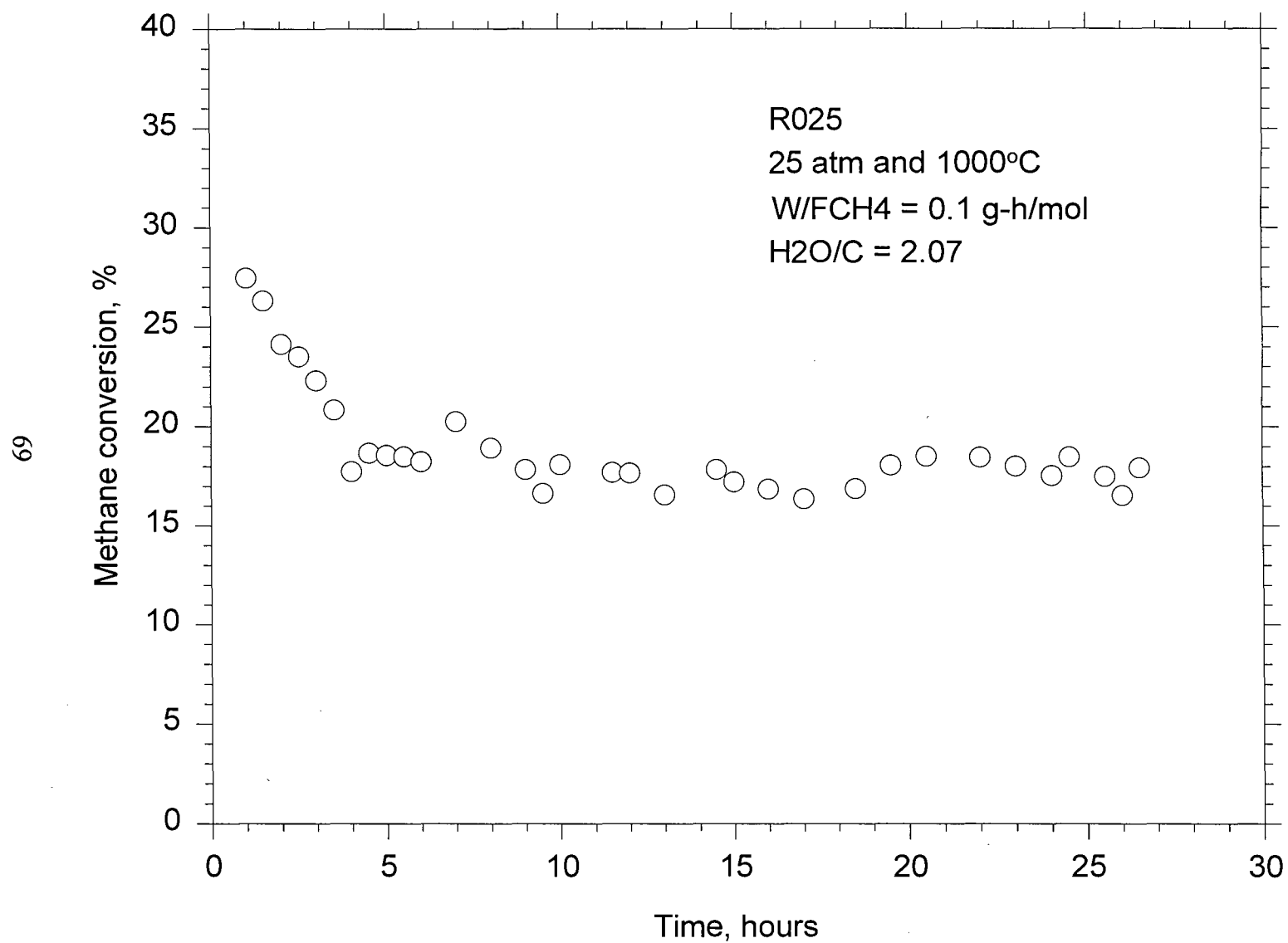
Figure 7. Stabilization of catalyst activity.
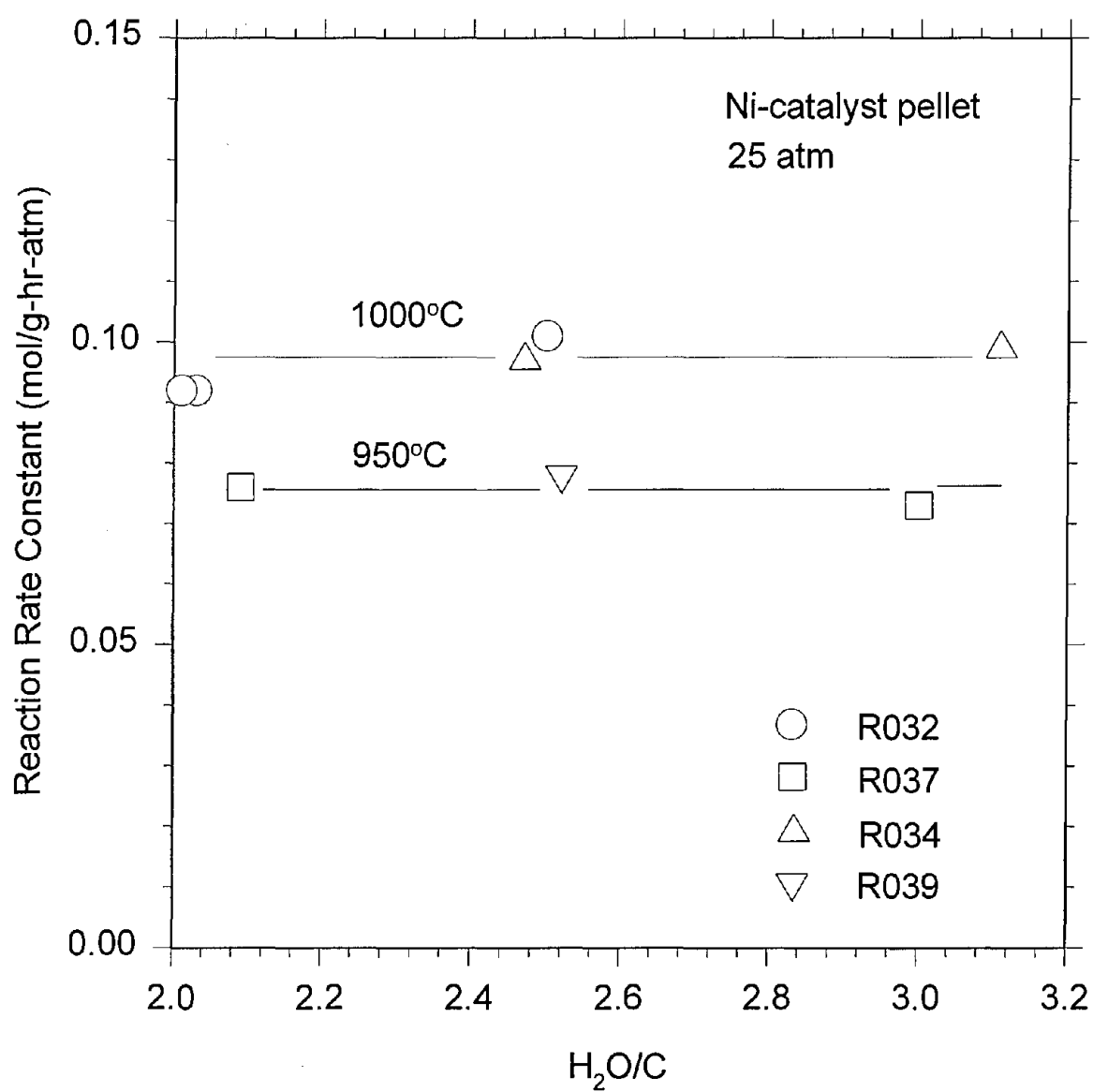
Figure 8. Effects of steam ratio on catalyst activity.
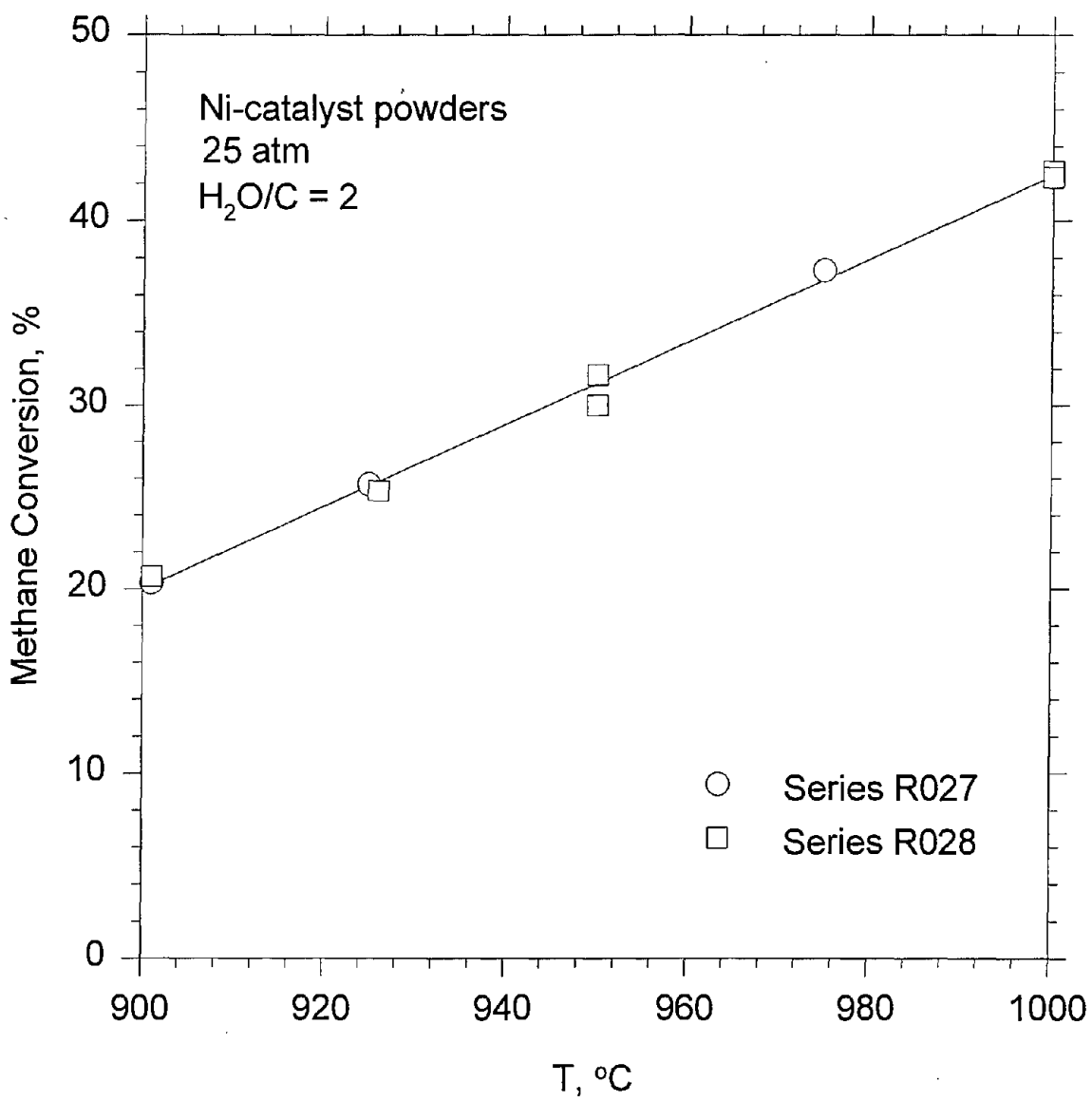
Figure 9. Effects of temperature on methane conversion
by catalyst powders.
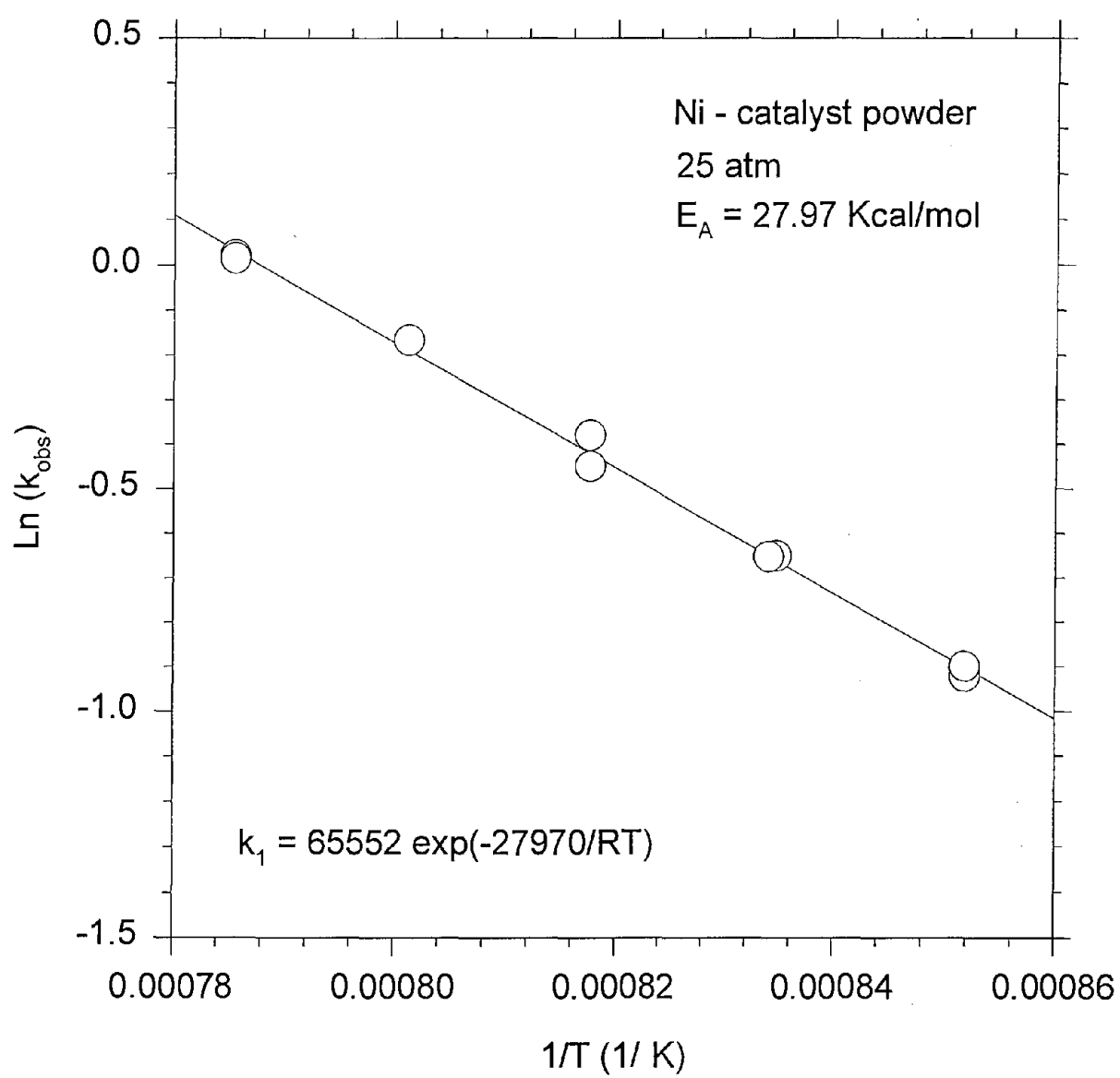
Figure 10. Arrhenius plot for catalyst powders.
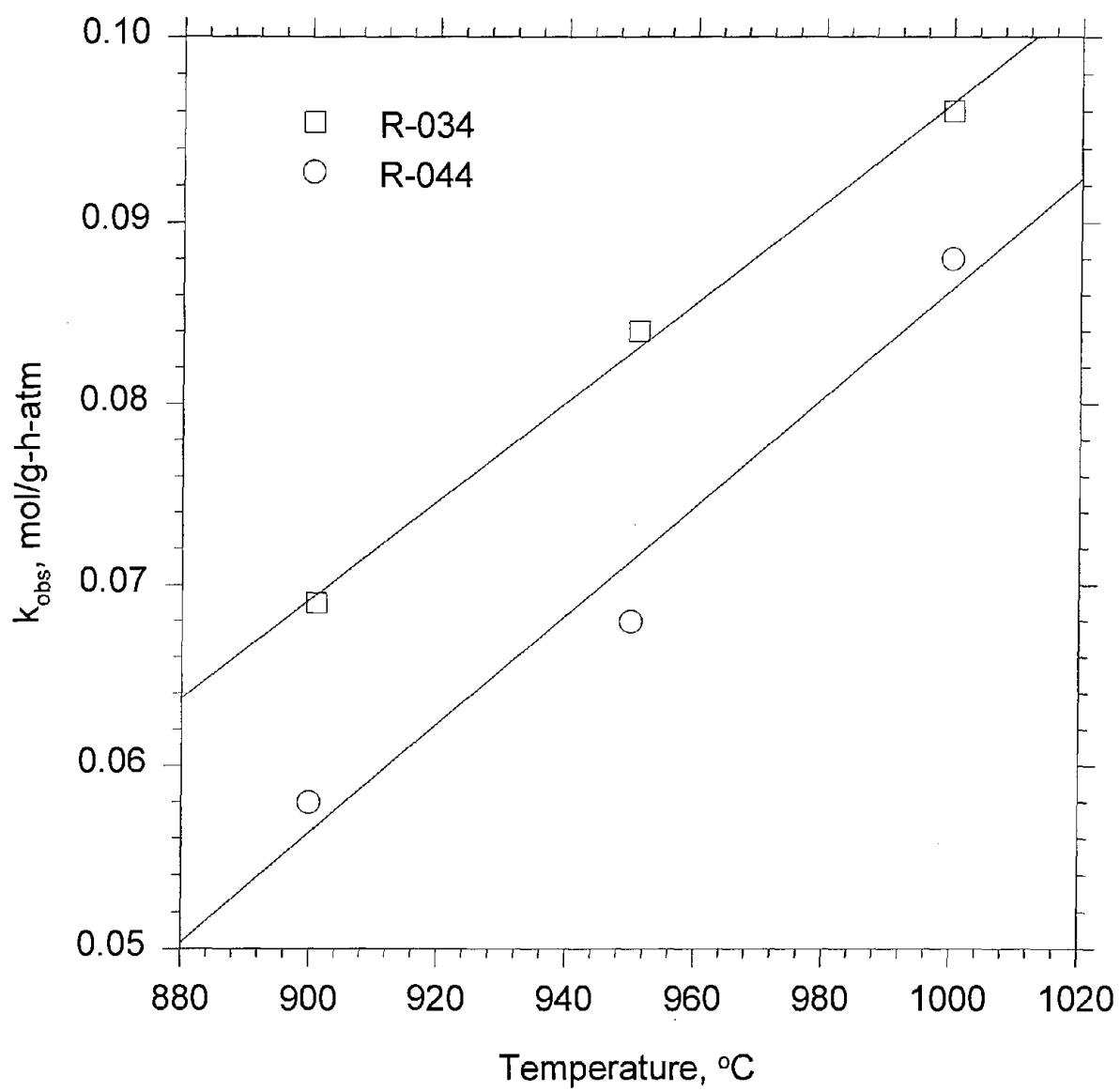
Figure 11. Activities of commercially sized catalyst pellets.
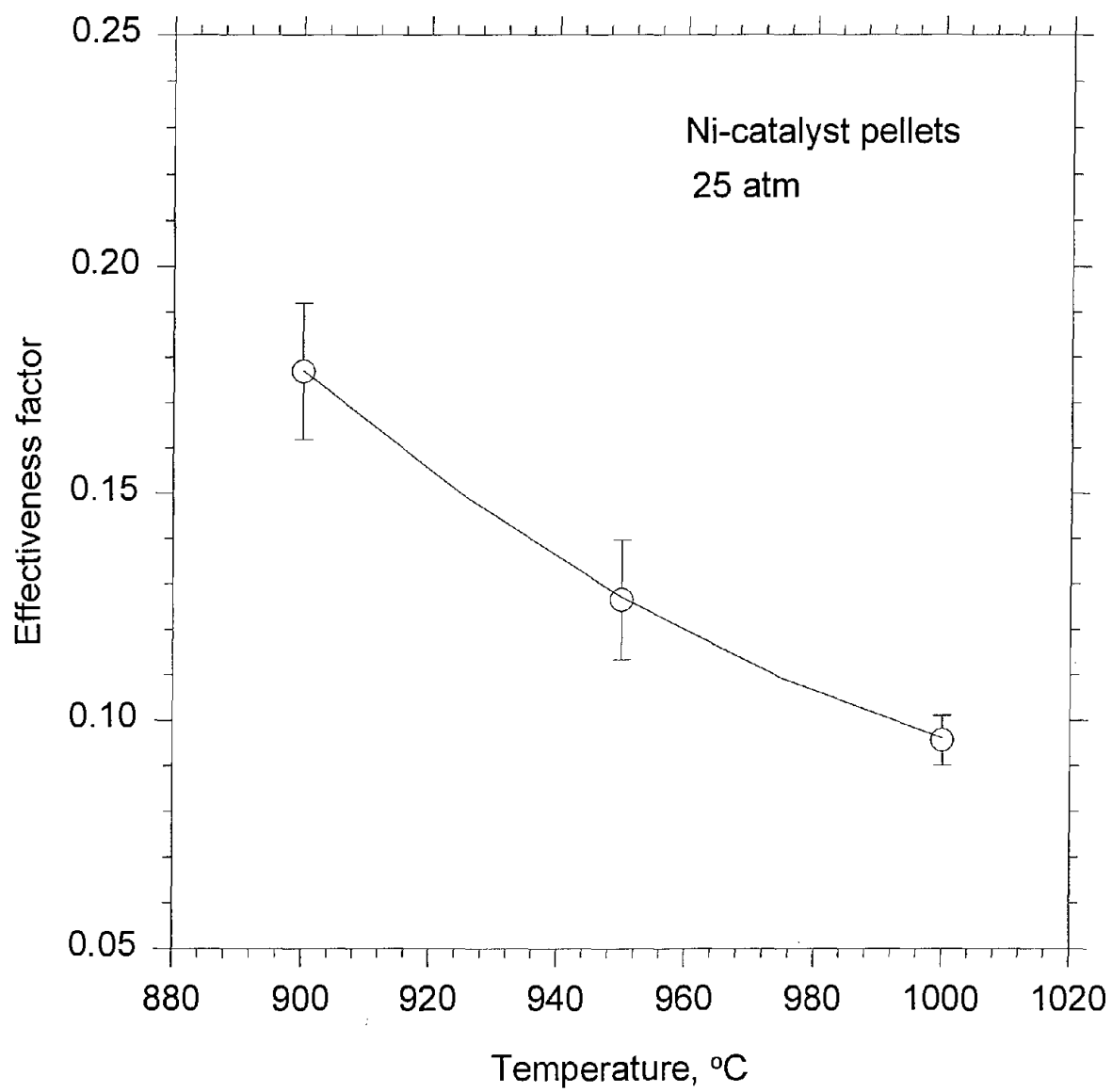
Figure 12. Effectiveness factors of catalyst pellets.
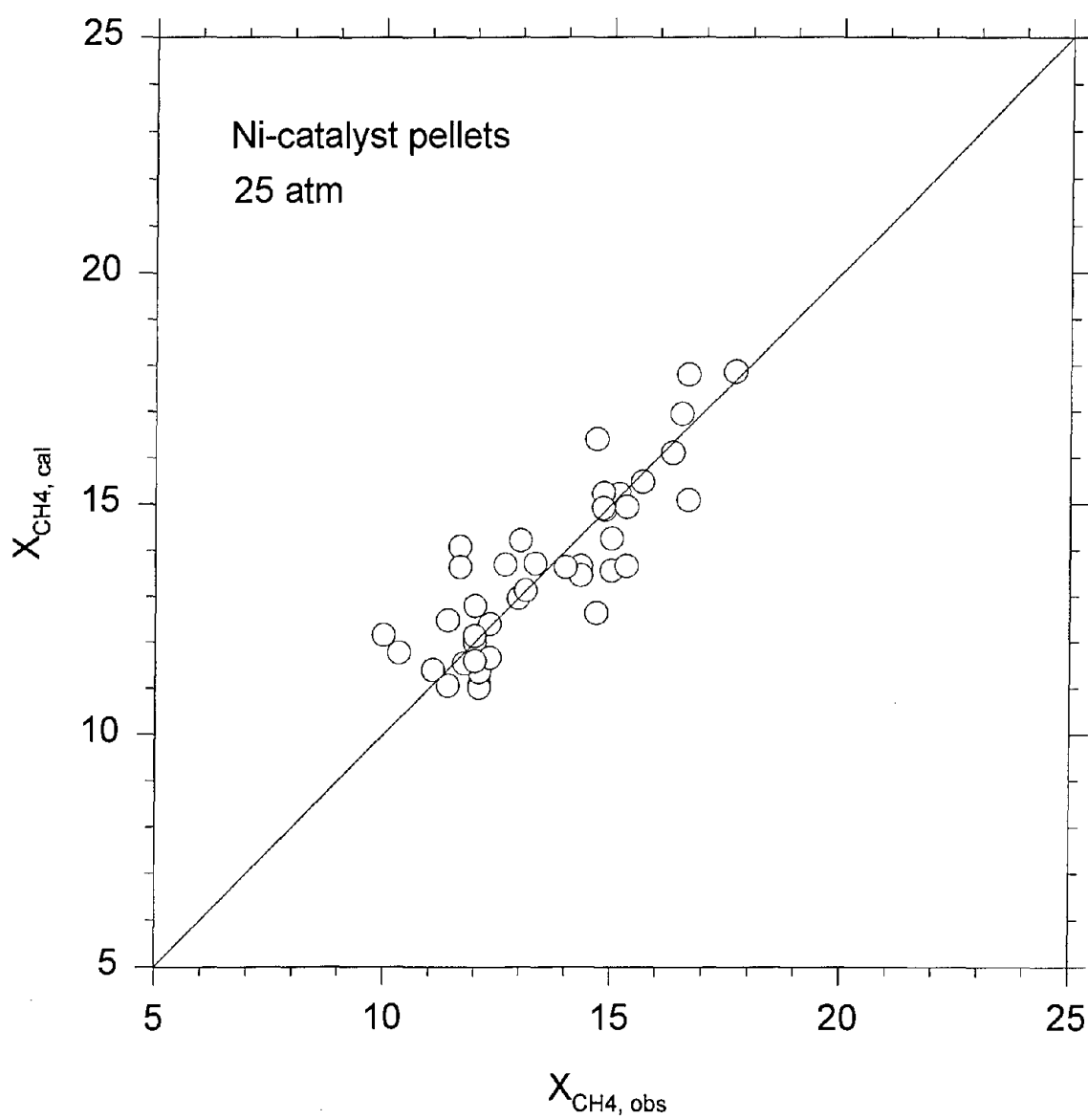
Figure 13. Comparison of calculation results with experimental methane conversion data.
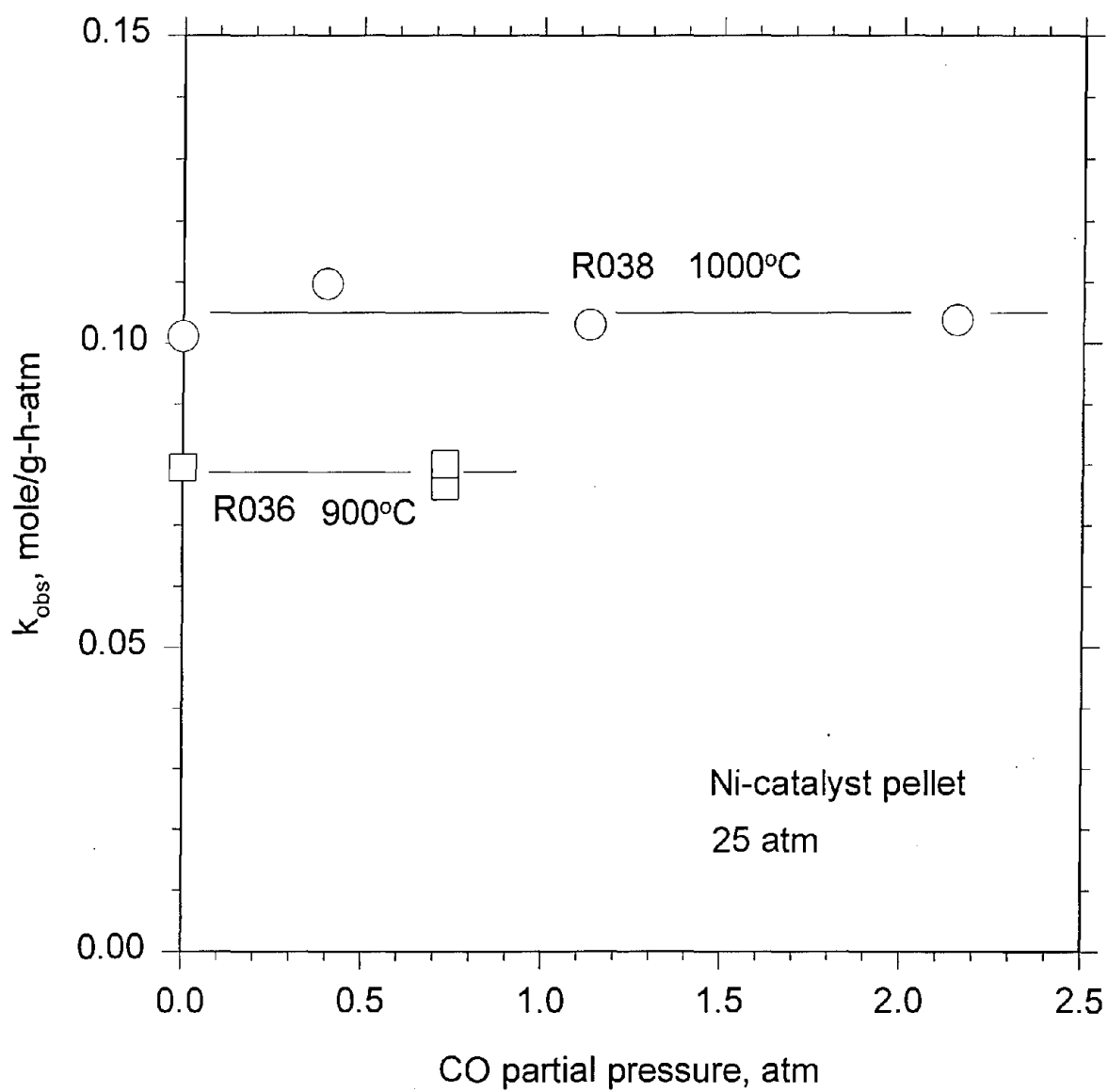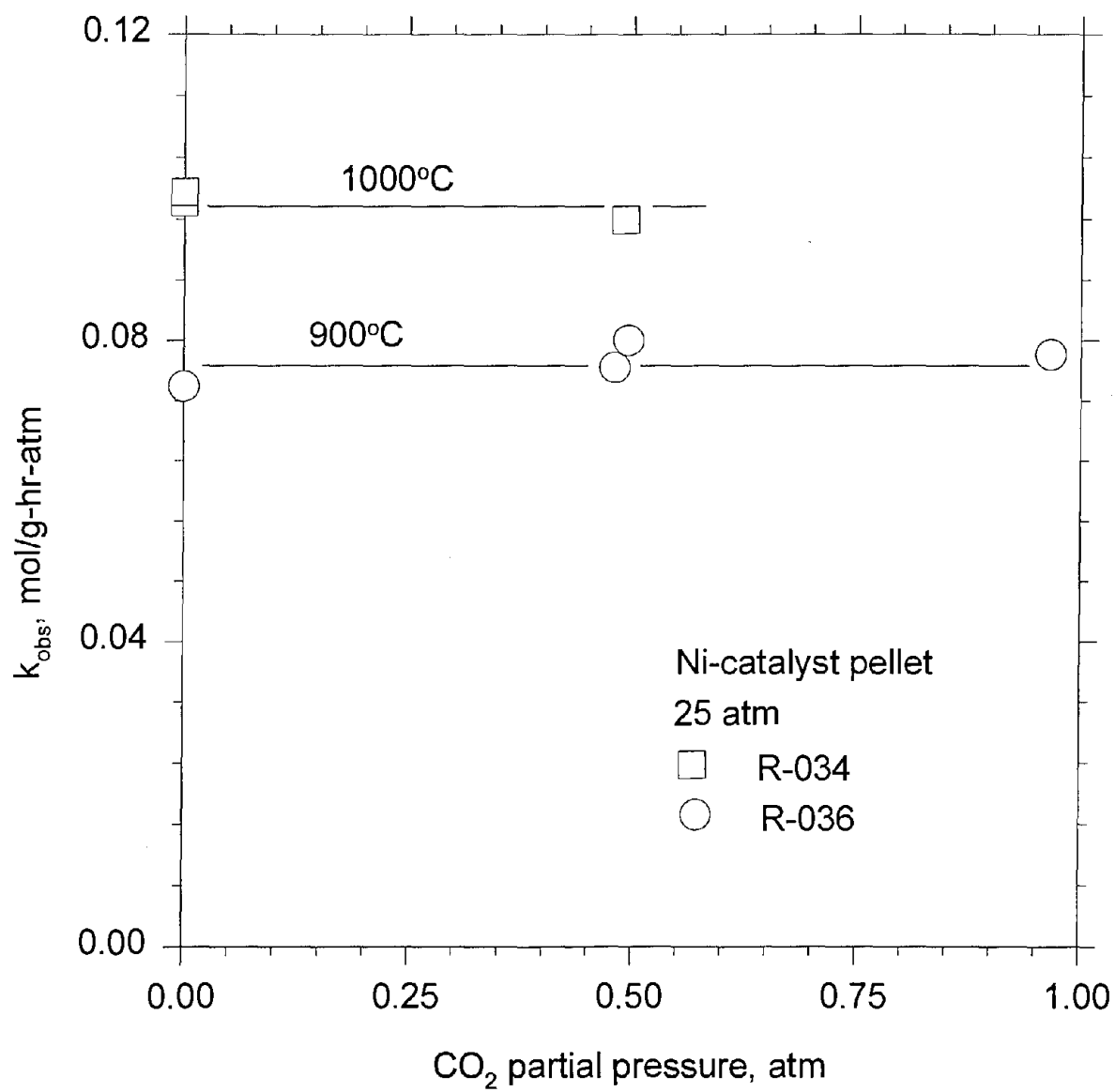
Figure 14. Effects of the CO partial pressure
in the feed gas on catalyst activity.

Figure 15. Effects of the CO_2 partial pressure
in the feed gas on catalyst activity.
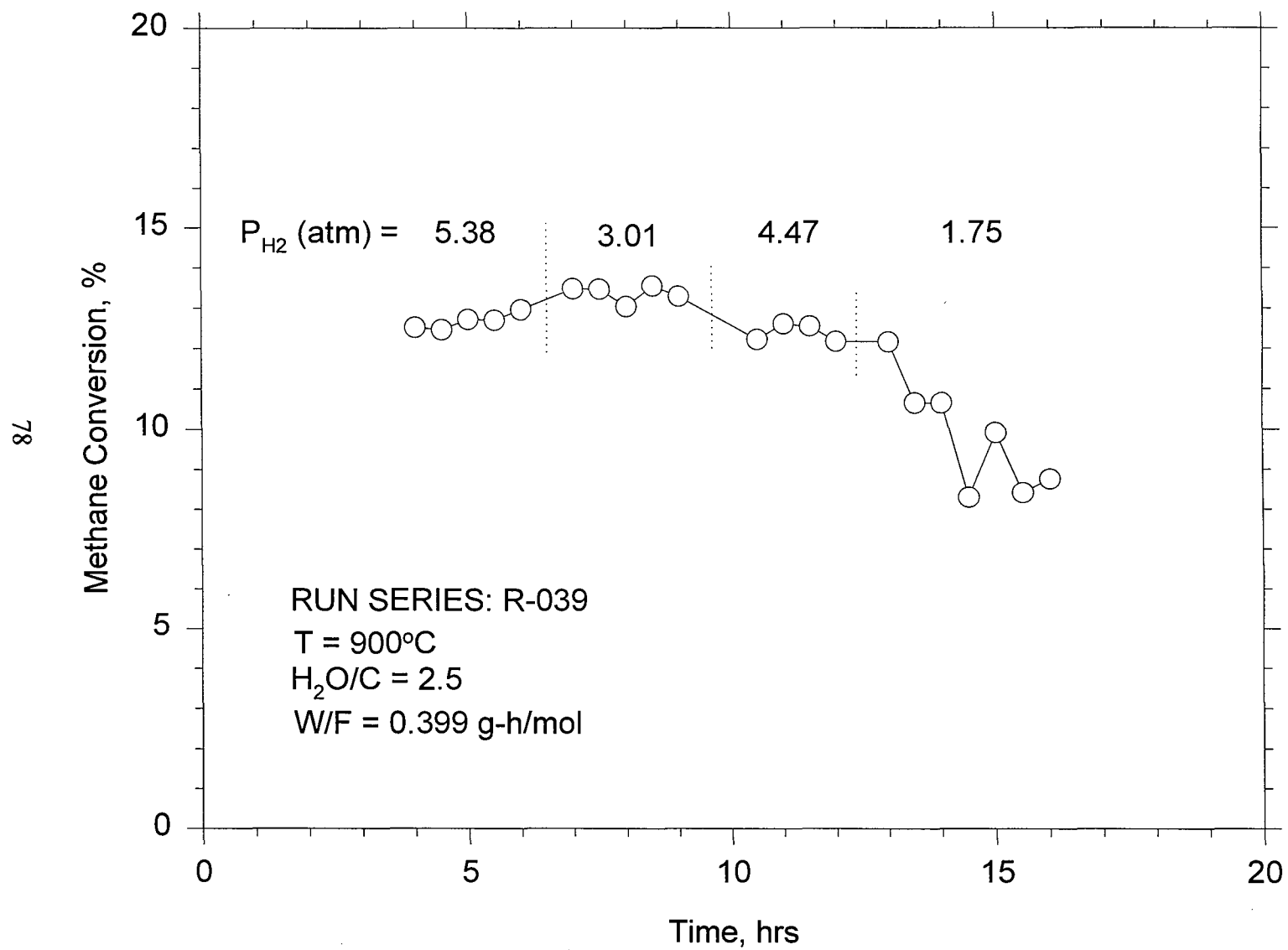
Figure 16. Effects of the H_2 partial pressure in the feed gas. (R039)
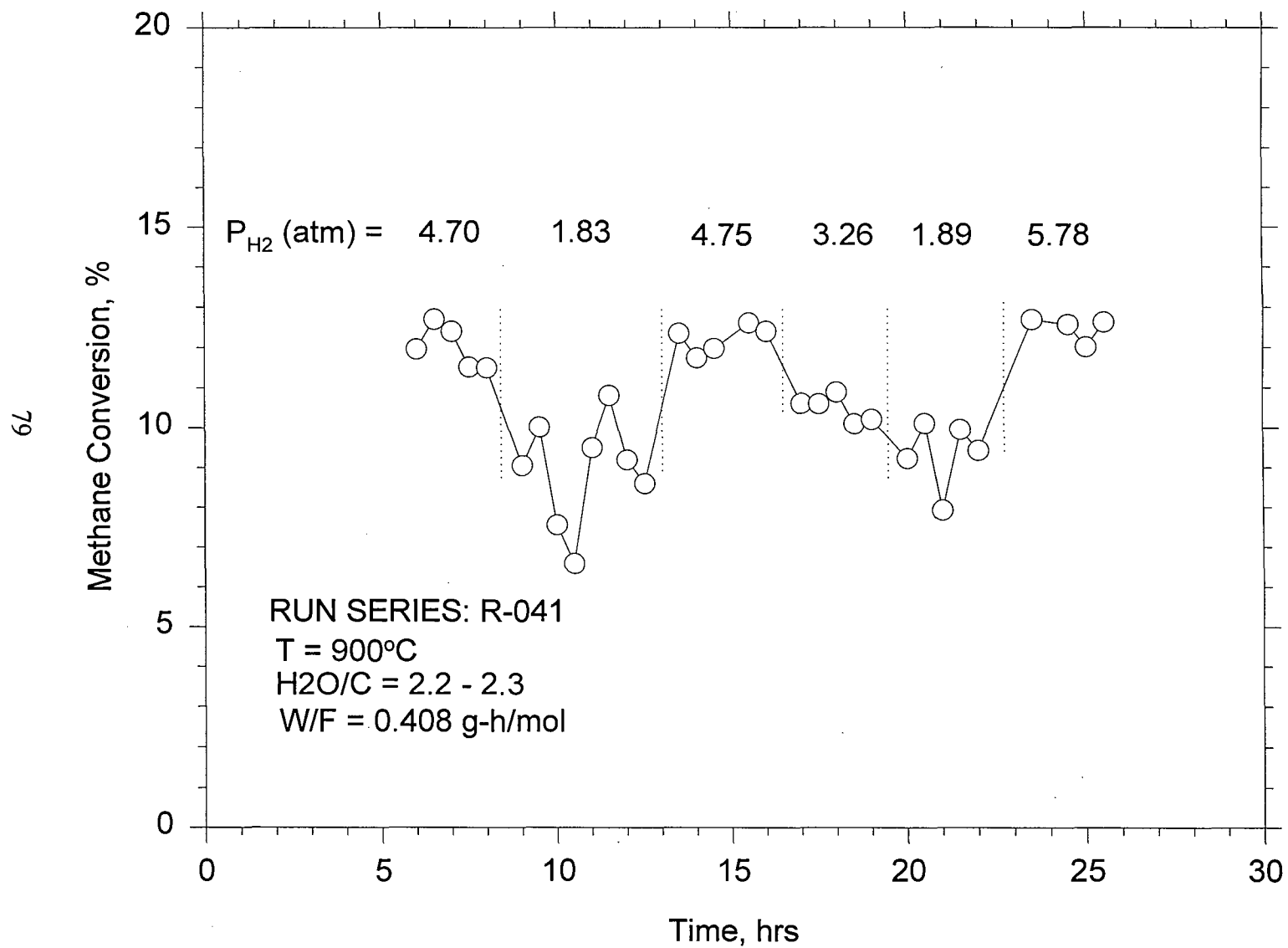
Figure 17. Effects of the H_2 partial pressure in the feed gas. (R041)
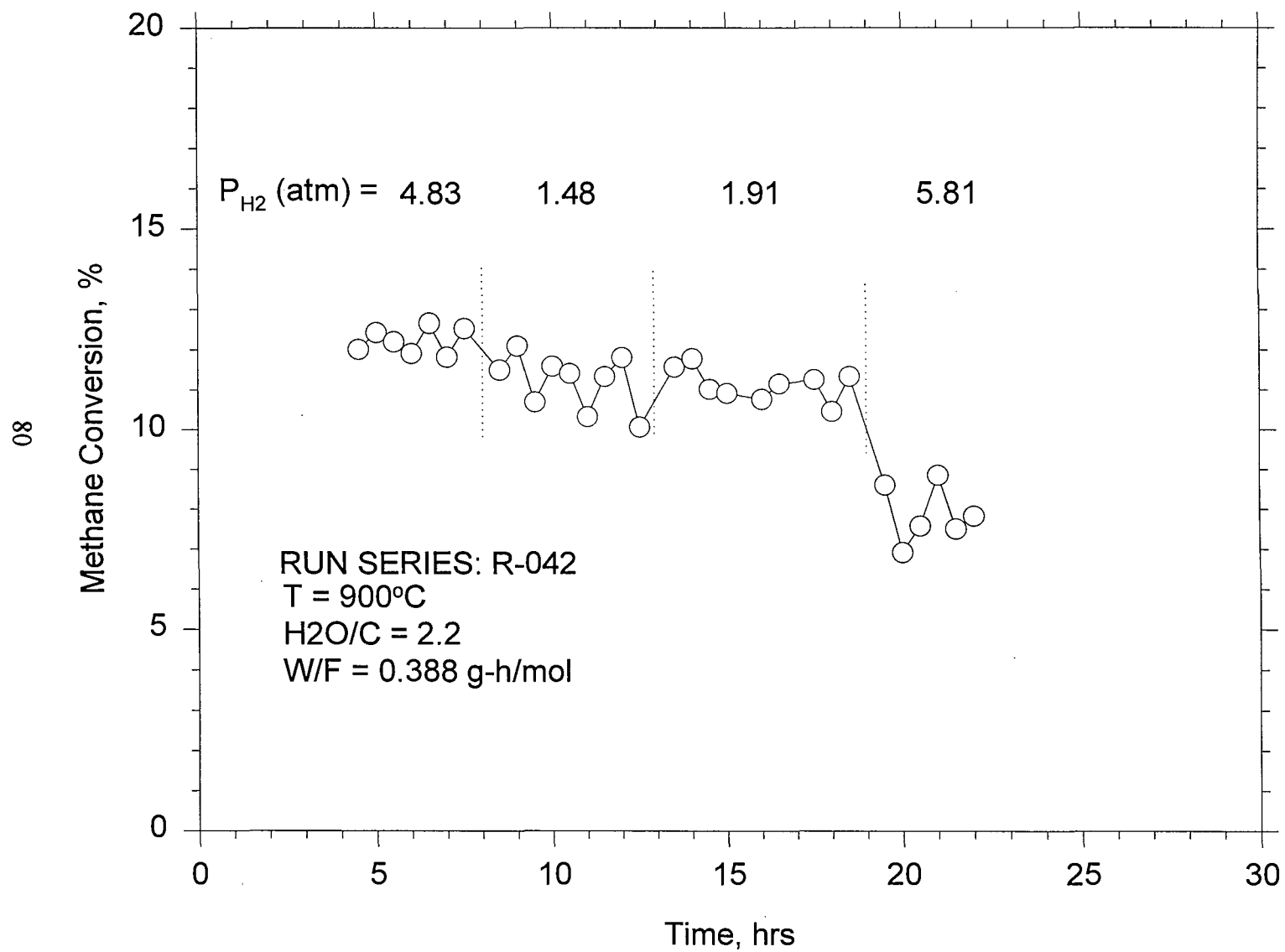
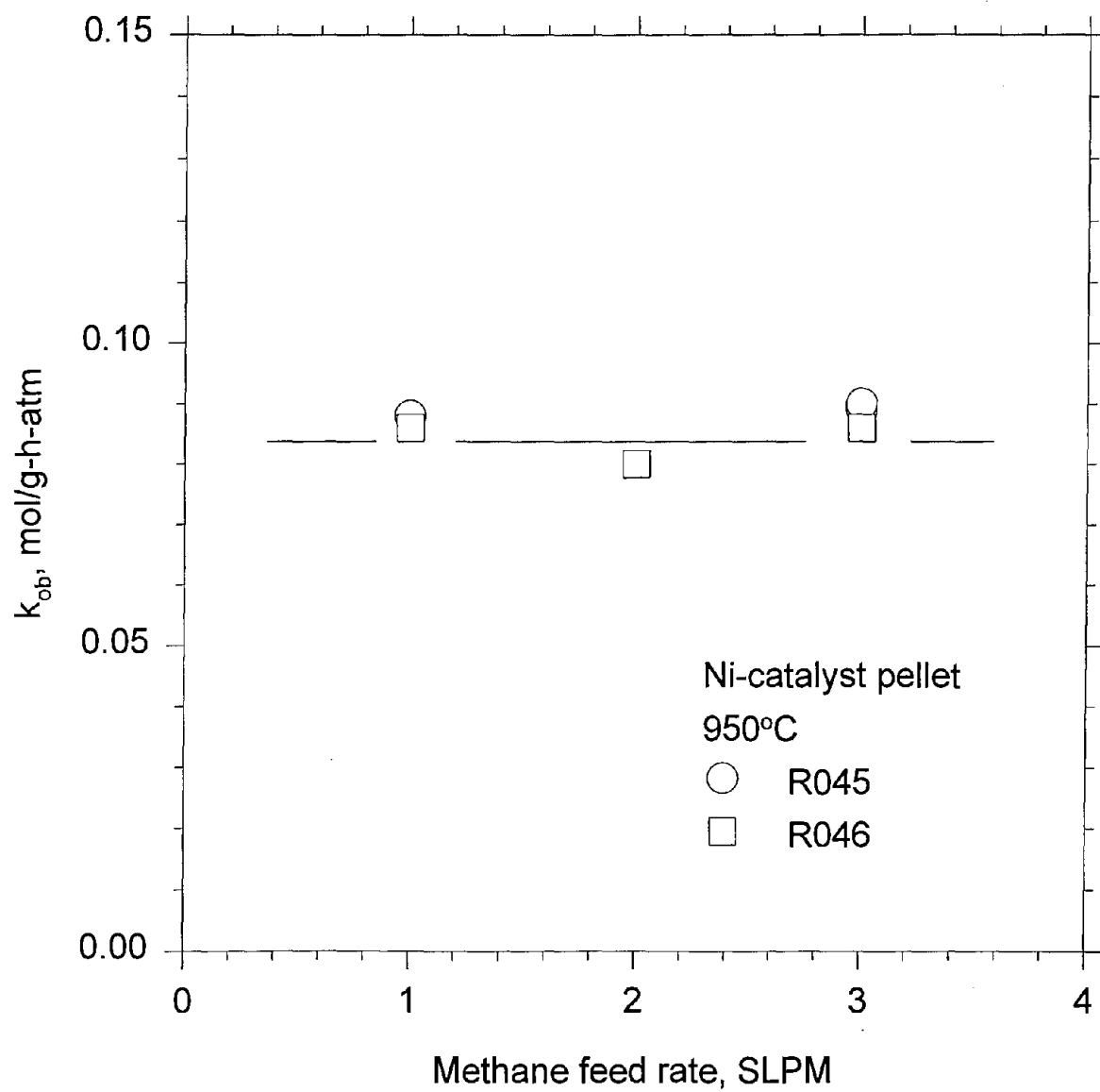Figure 18. Effects of the H_2 partial pressure in the feed gas. (R042)
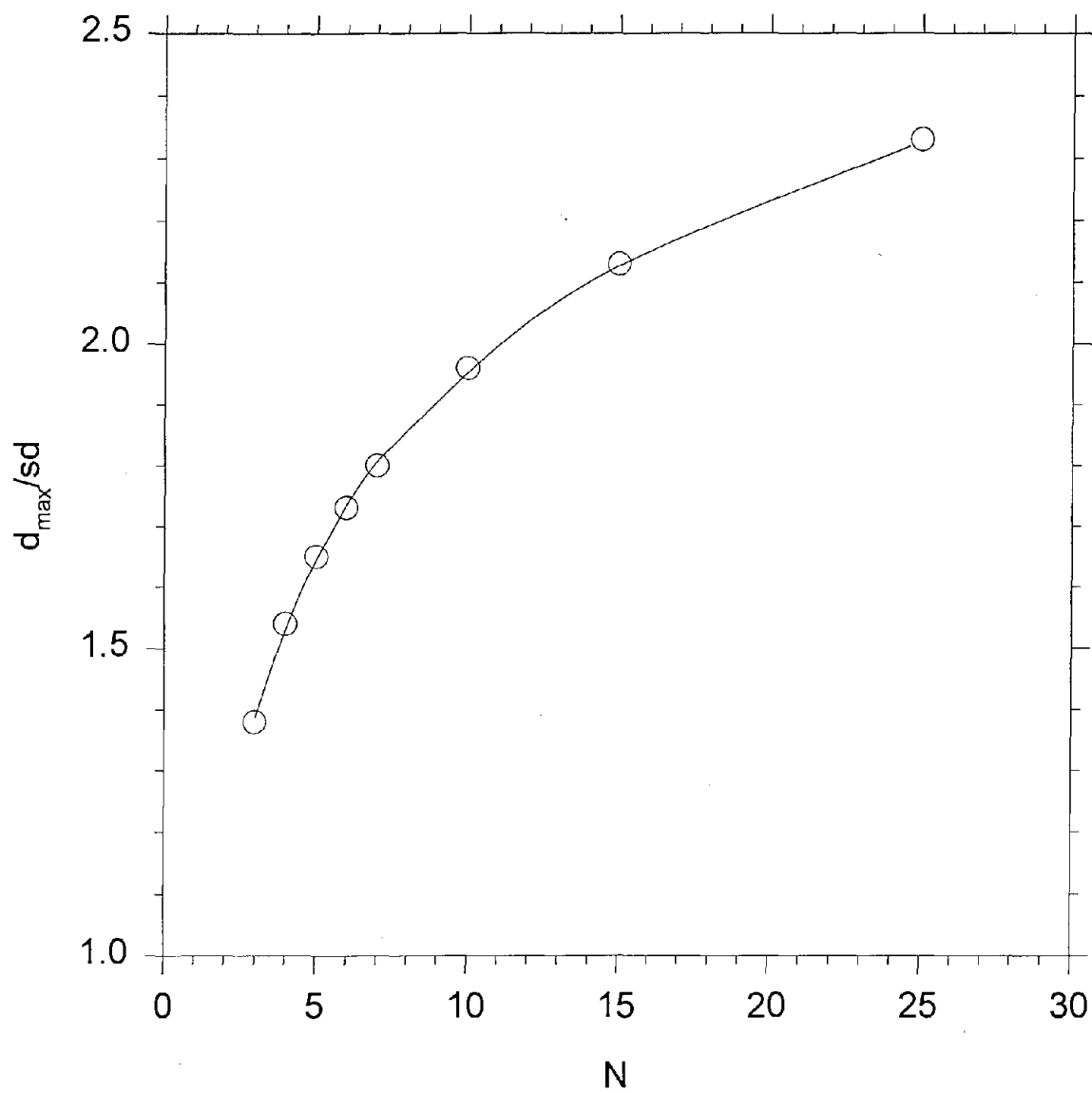
Figure 19. Constant k_{obs} observed at various methane feed rates.

Figure 20. Chauvenet's criterion for rejecting a reading.